FACULDADE DE ENGENHARIA DA UNIVERSIDADE DO PORTO

Deorbiting and Reentry of GAMASAT

Andrêa Corte-Real Albuquerque Costa

Mestrado Integrado em Engenharia Eletrotécnica e de Computadores

Supervisor: PhD Sérgio Reis Cunha

July 25, 2013

Resumo

A importância do envio de satélites para o espaço e de todo o desenvolvimento que isso implica, vai para além do que a mente pode imaginar. Diariamente fazemos uso das suas vantagens, sem se quer ser evidente. Estudos de imagens para previsões meteorológicas ou com um simples toque num recetor GPS ter disponível em poucos segundos o melhor caminho até ao destino, são alguns dos exemplos do proveito dos satélites. Dessa forma, há uma forte crença no retorno que o investimento no processo de desenvolvimento de satélites pode trazer em setores como saúde, educação, ambiente e segurança; as suas aplicações estão em constante crescimento. Assim, como qualquer evolução é necessário pôr à prova equipamentos projectados, o que implica a necessidade de enviar equipamentos para o espaço e recuperá-los. Dessa forma, é cada vez mais crucial investir e encontrar formas rentáveis e seguras de controlar a perda de altitude de satélites e até mesmo a sua reentrada, ou pelo menos, algumas das suas subestruturas destes.

O principal foco desta tese, inserido no projeto GAMASAT, é ajudar a dar um passo nessa direção. Nela será descrito o processo de desenvolvimento para um sistema de controlo da perda de altitude sem ajuda de propulsores e assim recuperar informação recolhida no período de orbita do satélite.

O projeto GAMASAT resultou de uma parceria entre a Universidade do Porto e a TEKEVER, para projetar o lançamento de um CubeSat abrangido pela missão QB50. O satélite irá conter uma cápsula que procederá à reentrada, juntamente com outros subsistemas, nomeadamente sistemas de: comunicação, navegação, determinação de atitude e equipamentos para efeitos de estudos atmosféricos.

Este projeto será desenvolvido em ambiente MATLAB, com o propósito de estudar a perda de altitude do satélite e a estabilidade da cápsula durante a reentrada. Para o desenvolvimento do sistema de controlo foram necessários estudos preliminares do coeficiente de arrasto a que o satélite estará sujeito e os seus efeitos na atitude. Este satélite será um modelo CubeSat 3U, capaz de controlar a sua órbita com o ajuste da área exposta ao vento aparente, recorrendo uso de rodas de inércia . O algoritmo de controlo iniciará o processo de atuação nas rodas de acordo com a informação recolhida do receptor GPS, visando sempre o ajuste da trajetória de reentrada para uma aterragem segura. Num dos compartimento do CubeSat encontra-se a cápsula que fará a reentrada, contendo os seguintes equipamentos: Transmissor de rádio SDR, outro receptor GPS, baterias, sensores e um actuador passivo *damping*. Para uma maior segurança, a aterragem dar-se-à no mar, mais especificamente na Zona Económica Exclusiva de Portugal e para auxiliar a sua localização e recolha as comunicações serão realizadas por mensagens UHF ARGOS.

Abstract

The importance of sending satellites to space and the implied developments goes beyond what the mind can reach. In our day-to-day lives there are a number of examples of its applications, such as weather forecast studies or to find the best route, with the touch of your fingers in a GPS receiver. Therefore, there is a strong belief that investement in satellites can be even more helpful and produce a direct impact on health, education, environment and safety. New applications for satellites are continuously arising. Some involve retrieving material back from orbit. For that purpose, it is absolutely essential to find new cost-effective and safe ways to de-orbit and re-enter satellites or parts of satellites.

The main goal of this thesis is to take a step in that direction and to describe the development of the de-orbiting control system without propulsion, followed by the capsule re-entry to recover that information, which will be performed in a GAMASAT project.

The GAMASAT project is a partnership between the University of Porto and TEKEVER, to launch a CubeSat enrolled with QB50 mission. This satellite will contain a re-entry capsule, together with other sub-systems: communications, navigation, attitude determination and equipment for atmospheric study.

This project will be developed in a MATLAB environment in order to study the satellite de-orbiting control and the re-entry capsule stability. In order to develop the control system for the de-orbiting, a drag coefficient study was primarily carried out, based on the satellite attitude. Being a 3U CubeSat, the de-orbiting control will be performed by reaction wheels that will change the exposed area to the ram direction. The control algorithm will cause actuation according to the navigation data from a GPS receiver and aims to adjust the re-entry trajectory towards reaching a safe landing area. The capsule that contains a SDR radio transmitter, another GPS receiver, batteries, sensors and a passive damping actuator will perform the re-entry. The landing will occur on the sea, more exactly on Exclusive Economic Zone of Portugal, and for its recovery the communication will be performed through UHF ARGOS messages for location determination.

Acknowledgments

I realized that I do not know where to begin. So, I just wanted to say that what I made it, I made it because all of you gave me the best of you guys. All of the pushes, the laughs and the supportive words did not made the things easier, but it made me not lose the forces. Thank you, thank you for the patience, thank you for the help, thank you for smiles, thank you be here or on the other side of the line. Writing your names here is just a small gesture that I found to show my appreciation for all of you have done, but was the way that I found to let you know that what you have done I will never forget. To all of you, Thank you:

António Côrte-Real

Kátia Miotelo

Mariana Santos

Margarida Carvalho

Nuno Sousa

Sérgio Reis Cunha

Susana Rafael

Tom Segert

"Human beings are divided into mind and body.
The mind embraces all the nobler aspirations, like poetry and philosophy,
but the body has all the fun."

Woody Allen

Contents

List of Figures

List of Tables

Abreviaturas e Símbolos

ADCS	Attitude Determination and Control System
DASA	DaimlerChrysler Aerospace
DEEC	Departamento de Engenharia Electrotécnica e de Computadores
EADS	European Aeronautic Defence and Space Company
EEZ	Exclusive Economic Zone
ESA	European Space Agency
e.g	*exempli gratia* for example
LEO	Low-Earth Orbit
FEUP	Faculdade de Engenharia da Universidade do Porto
GPS	Global Positioning System
IAA	Independent Academies Association
ISS	International Space Station
IRDT	Inflatable Re-entry and Descent Technology
IRVE	Inflatable Reentry Vehicle Experiment
JAXA	Japan Aerospace Exploration Agency
LEO	Low Earth Orbit
NASA	National Aeronautics and Space Administration
TLE	Two-Line Element
SDR	Software Defined Radio
YES 2	Young Engineers' Satellite 2
WWW	*World Wide Web*

Constants

m	Mass
g	Gravity Acceleration (9.8 $\frac{m}{s^2}$)
ρ	Air density
ρ_0	Nominal Density
λ	Wavelength
A	Area
Cx	Drag coefficient
R	Universal Gas Constant (8.31 $JK^{-1}mol^{-1}$)
M_{mol}	Molecular weight
n	Number of moles
T	Temperature
P	Pressure
p0	Nominal pressure
dA	Infinitesimal area
dz	Infinitesimal heigh
V	Volume
h	Altitude
H(z)	Scale Height
Al	Albedo
σ	Stefan–Boltzmann constant ($5.670373(21)10^{-8}Wm^{-2}K^{-4}$)
F_D	Drag Force
Δv	Velocity variation
M_C	Capsule mass
V_{DV}	Volume displaced
ρ_{sea}	Sea density ($\approx 1g/mL$)

Chapter 1

Introduction

The GAMASAT is a project aimed at building a CubeSat to be launched into Low-Earth Orbit (LEO). It is estimated to stay in orbit for a estimated period of three months. During this time it will be used to conduct an experiment focused on measurements that will help to know and understand more about the lower thermosphere and ionosphere. The measurements will be backed up in a flash memory protected by a capsule inside the satellite. This capsule will be released from a 3U CubeSat, to re-enter through the Earth atmosphere. It is planned to splashdown on the sea, in the Portugal Exclusive Economic Zone (EEZ). Returning a capsule using a CubeSat has not been done before. It involves a great deal of uncertainty owing to the consideration of its integrity and impact zone.

This thesis present a control architeture system to adjust the de-orbiting of the CubeSat so that the realesed capsule performs re-entry in a way such that the splashdown area is compliant with the Portugal EEZ.

The main idea of the de-orbit control is to perform differential drag during re-entry. This is achieved by positioning different sized sides into flight directions using reaction wheels inside the satellite.

This thesis also focuses on the re-entry itself, adressing the problem of the re-entry capsule stability. For that a design of capsule structure and oscillation dumping mechanism is presented.

1.1 Project organization

This thesis consists of seven chapters. The first two comprise an overview of the whole project. In it the main goals become apparent, as do the working plan, the approach chosen to solve it, the tools that will be used and what the state of the art. The third chapter handles the first stage regarding the theme of this thesis, the satellite de-orbiting. This chapter aims to analyses the conditions and the attitudes of the satellite in LEO. The fourth chapter presents an algorithm control and the conditions required to activate the controller and simulation for the de-orbiting algorithm control. The fifth chapter showcases the requirements and the capsule design. After,

chapter six analyzes its (un)stability during re-entry. Following by the chapter seven that suggest a future works .

1.2 Project Schedule

The analysis and the algorithm control play a very significant role in the success of this project. Therefore it is crucial that careful planning of resources is done.

This thesis will be lined up bearing in mind the following topics.

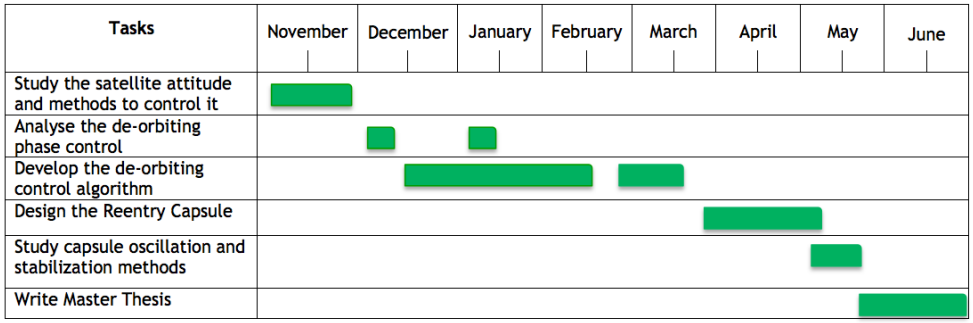

Figure 1.1: Work Plan

Chapter 2

Project Overview

The following chapter will give a general overview of the context of this project, a description of the project itself, and demonstrate how this thesis will fit the GAMASAT goals.

2.1 CubeSat

The CubeSat is a successful project in university research. Due to their dimension these satellites are an affordable way of research for the university level.

A CubeSat is a nanosatellite with standardized dimensions. It as the shape of a cube, with 1U (10x10x10 cm), and weighs around 1 kg. Larger structures can be achieved by assembling multiple units of 1U (e.g 2U : 20x10x10 cm or 3U: 30x10x10 cm).

This type of miniaturized satellite was developed in 1999 by Dr. Bob Twiggs and Dr. Jordi Puig-Suari, with the purpose of enabling graduate students to be able to design, build, test and operate a spacecraft in space. Nowadays, because of its simplified design, almost anyone can build them, and the instructions are available online, and for free.

It has become popular among schools and governments because of its low-cost and because it is so easy to built it.

In order to reduce space debris, they are usually placed in low orbits and fall back on earth within a few weeks or months.

2.2 QB50 Project

Project QB50 has a scientific mission to study *"in situ the temporal and spatial variations of a number of key constituents and parameters in the lower thermosphere"* [1] throughout the launching of 50 CubeSat, in 2015. The 50 satellites will collect data independently, for a period of 3 months, and will be also provided a study of the re-entry process.

From many points of views, the study of the lower thermosphere has shown to be the ideal choice for CubeSat developers, as the mission sees a decrease in time of measuring (3 months), which is below 330 km, and there is no risk of collision with the International Space Station (ISS).

The reduced distance with LEO allows high data rates and is below the Earth's radiation belts, which reduces the cost.

Owing to the drag coefficient, up until re-entry, the CubeSats will decay and slowly pass through all the thermosphere allowing enough samples for the study.

2.3 GAMASAT

GAMASAT is a project developed in cooperation between TEKEVER and the University of Porto, to launch the first Portuguese CubeSat.

GAMASAT will have a 3U dimension. Part of it will be reserved for the study case of QB50 project, and the other will lodge the capsule developed between both entities.

GAMSAT encompasses two major experiments. The first one has a technological focus, using of Software Defined Radio (SDR) to "establish and exploit an ad hoc network with satellite-to-satellite and satellite-to-ground link, to provide larger data volume throughput, reception of GPS signals and attitude determination using radio waves"[2]. The second one, which will be explored in this thesis, consists in the controlling of the de-orbiting phase of the CubeSat and also the capsule release to begin the re-entry process.

This project will be developed in a MATLAB environment and in Solidworks for the re-entry capsule design.

2.4 Challenge Approach

Since the focus of this thesis is to explore the control of the satellite de-orbiting and ensure a safe recovery of the capsule, it will explore the following items: de-orbiting, actuation range, algorithm control capsule release and finally the capsule re-entry and splashdown.

2.4.1 De-orbiting

The approach for the de-orbiting control of the 3U GAMASAT is to periodically actuate on the drag force by atittude control, based on a continuously running landing point forecast algorithm, and then release the capsule shortly before re-entry. The control will be made according to the navigation data obtained from GPS and targets a short list of re-entry points that ensures safe landing. The Attitude Determination and Control System (ADCS) will maintain the CubeSat aligned with the velocity vector within an error envelope of 5° with the science payload facing

the apparent wind. Once it reaches below 200 km and until the 110 km, specific reaction wheels will change the area of the satellite exposed to the ram direction, allowing to change the ballistic coefficient with a factor of 3, in a few seconds.

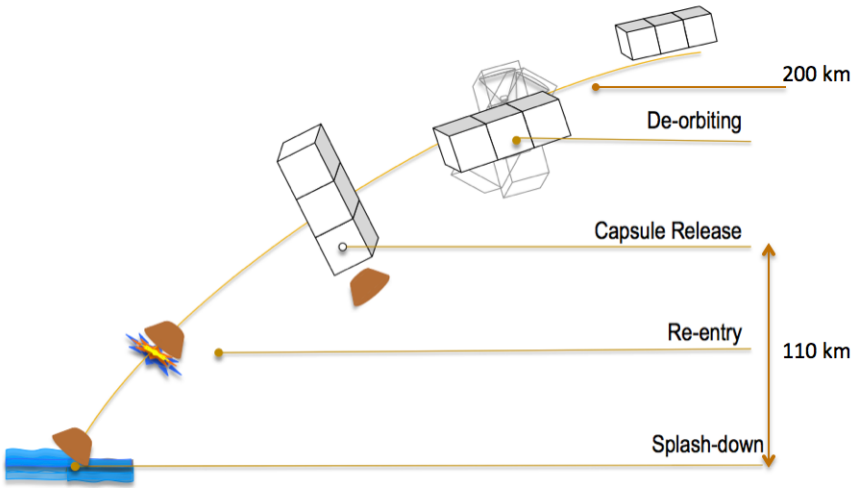

Figure 2.1: Re-entry phases

The return of any satellite involves a great deal of uncertainty in what concerns its integrity and impact zone accuracy. The challenge of GAMASAT is to design a simple system for satellite re-entry, defining the impact zone. It is important to choose an impact zone that guarantees safety and yet makes recovery still possible.

To understand the impact zone selection, the following expression gives the kinetic energy of a free falling object on the surface of the Earth:

$$E = \frac{m^2 g}{\rho C x A} \tag{2.1}$$

Where m represents object mass, ρ represents air density at MSL (roughly 1,2 kg/m^3), $\boldsymbol{g}$ represents gravity acceleration (9,8 m/s^2), $\boldsymbol{A}$ the area of the capsule exposed to the apparent wind (about 64 cm^2) and $\boldsymbol{Cx}$ is the drag coefficient at terminal velocity and at MSL (estimated to be around 0,8).

The re-entry spot needs to guarantee the safety and accessibility to allow for its recovery. For an object's landing to be considered safe on the ground, its energy is limited to 15 J. A capsule with 0,1 kg has an estimated kinetic energy of around 15 J, which is too close to the limit. Since in this project the capsule will have about 0,2 kg, the algorithm will assume a re-entry with splashdown on water. Therefore it is planned to land within the Exclusive Economic Zone (EEZ) of Portugal exclusive of the Atlantic.

2.4.2 Actuation

Active control of the satellite will occur between 200 km and 110 km. The following chart can help understand the altitude range were it make sence to preform re-entry control.

The blue line represents a simulation of the along track variation of the landing point given a +/- 50% drag force variation relative to standard conditions (either due to attitude or air density variation), in units of orbits.

The red line represents the remaning flight duration, in units of hours.

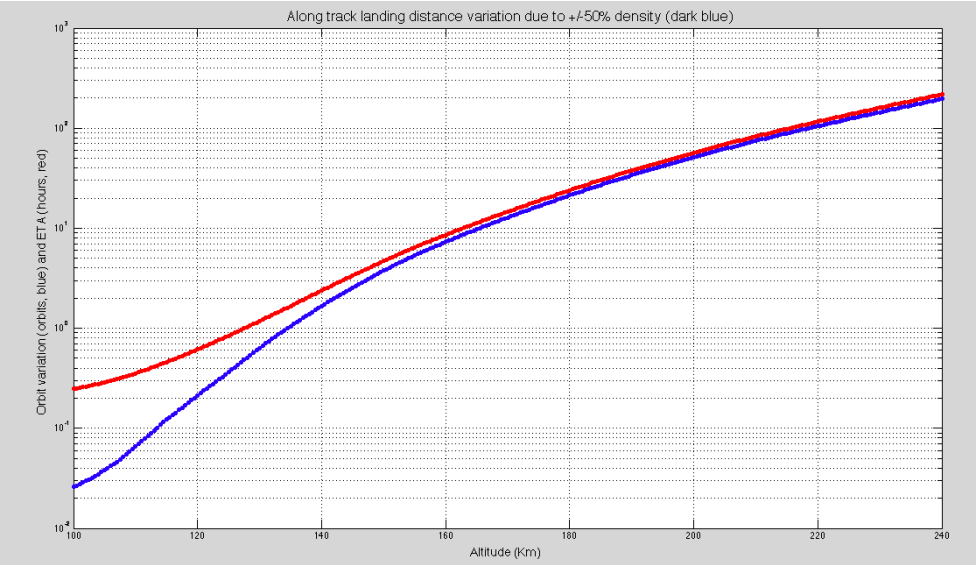

Figure 2.2: Distance variation with +/- 50% density variability

Above 200 km the uncertainty is still too high for it to be worth spending control energy, whereas below 110 km the capsule landing region variability is already limited to 500 km along track, and the satellite is just a few minutes from re entry. Cross-track variability is an order of magnitude lower than a long-track variability.

Actuation will occur in cycles of 30 minutes, each cycle initiating with a new GPS reading. For energy consumption management, the onboard GPS receiver will be operated temporally, having been determined that 30 minutes intervals between observations is adequate to maintain a suitable ephemeris (the satellite will periodically computes and broadcast its own ephemeris in the format of Two-Line Element (TLE) [21].

One of the larger faces will be exposed to the apparent wind during a T_{on} time interval and then the satellite will be returned back to the normal attitude (smaller face aligned with the apparent wind). This rotation will occur below 200 km until the 110 km, specific reaction wheels will change the satellite exposed area in a few seconds and adjust the ballistic coefficient with a factor of 3.

Adjusting the duty cycle (T_{on} against the duration of the cycle) allows to actively control the re-entry location. In order to perform such rotation in a short amount of time, specific reaction

wheels will be employed. These will have significant actuation effectiveness, but low accuracy, since upon rotation the Attitude Determination and Control System (ADCS) will perform any required fine-tuning.

2.4.3 Control Algorithm

The magnitude of T_{on} will be computed at the beginning each cycle, by the algorithm that uses the information collected from the updated TLE and predicts the landing spot. A simulation routine computes a landing location for given T_{on} and given density variations of the atmosphere. This algorithm assumes that the T_{on} intervals have an average value of 25% for the following cycles and that the capsule is released at 110 km. This algorithm results from simplifications of more elaborate procedures, yet giving a sufficiently accurate forecast. It also includes some corrective parameters that will increase accuracy based on previous data.

The optimal T_{on} is chosen as a way of minimizing cost function that includes a blend of average landing (stochastic solution) and also a worst-case scenario for the possible drag variations.

2.4.4 Re-entry capsule

The re-entry capsule will be release from inside the satellite, with a shape designed for re-entry. Built using a heat-resisting materials, this capsule will have a minimal payload, consisting of a radio transmitter, battery and basic sensors (temperature, acceleration and rate of turn). It will also have an off-the-shelf miniature GPS receiver to be used after the deceleration phase of re-entry and upon falling into the ocean.

The capsule will have the general shape similar to the successful Apollo 11 used in one of the lunar missions by NASA, with a 9.5 cm diameter and height about 5.5 cm. It will weigh about 0.15 kg, most of it due to the ceramic material that will protect the interior with little ablation. A cork composite ablative material will cover it. Inside the capsule there will be:

- An oscillation dumping mechanism;
- Batteries;
- Antennas (2,45 GHz and 402 MHz);
- ARGOS Antenna;
- Flash memory with extensive GAMASAT flight data;
- Microcontroller;
- GPS;
- Solar Panel;
- Flash Light;

- Infrared;
- Temperature, acceleration and gyroscopic sensors.

Chapter 3

State of the Art

This chapter present a brief review on previous works and studies about de-orbiting and re-entry.

3.1 Overview

In the past a number of experiments for de-orbit and re-entry of small and medium sized objects have been performed by the major space agencies.

These experiments can be classified into the following approaches:

Miniaturized Apollo style capsules

- Hayabusa
- YES 2

Deployable Re-entry Capsules:

- IRDT
- NASA inflatable

While the miniaturized Apollo style capsules aim at equipping smaller systems with de-orbit capability, the deployable re-entry capsules aim to allow a medium sized system to bring down even more payload by reducing the mass and volume fraction of the de-orbit device.

Another method to differentiate between the re-entry systems is the method of de-orbit control. While the larger and often more sophisticated capsules like IRDT focus on a classical propellant based re-entry control system this option is often not feasible for the smaller capsules. The following different methods have been used:

Propellant based re-entry control

- Inflatable Re-entry Demonstrator Technology (IRDT)
- NASA inflatable
- Hayabusa

Teather supported re-entry control

- YES2

The method of differential drag de-orbit control has been proposed but not yet been implemented [3]. Therefore while being comparatively conservative on the actual capsule design the GAMASAT project will excel beyond the state of the art mainly on the field of re-entry control.

3.2 Description of Existing Systems

In the following section the performed experiments of the existing capsules as well as those under development will be explained in more detail.

3.2.1 Inflatable Re-entry Demonstrator Technology - IRDT

Originally the IDT was developed for Russian Mars96 mission. Unfortunately it was lost due to upper stage failure of the mission. The DaimlerChrysler Aerospace (DASA) (an European Aeronautic Defence and Space Company (EADS) predecessor company) and Russian Space Company Lavochkin made an agreement in 1998 to commercialize the technology for earth applications. Two experiments were conducted. Unfortunately the two demonstrator flights in 2000 and 2001 were again not successful. The basic idea behind the IRDT was to test the concept of an Inflatable Re-entry Demonstrator. Its aim was to validate the function to enable the re-entry in a small, lightweight and cost-effective way. It was done using an inflatable extension system. This system offers an increase of ratio between volume and mass and is thus able to perform deceleration to take place in higher (less dense) areas of the atmosphere which will in result decrease both the mechanical as well as the thermal loads acting on the capsule.

Purpose: The purpose of the project was to design and built a re-entry capsule, that could remain in orbit for a longer time during the re-entry process would reduce dramatically the speed until it lands.

Who: The Inflatable Re-entry and Descent Technology (IRDT) is project developed by the European Space Agency (ESA), Russian aerospace company Lavochkin and DASA, launched into a sub-orbital ballistic re-entry trajectory by the space launch rocket, Volna, fired from a Russian naval submarine positioned in the Barents Sea in the area of Severomorsk, Russia.

What: The IRDT is a re-entry capsule that increases it diameter during the re-entry. The increase in size was made using an inflatable extension of the cone in two stages. This procedure allows a slower re-entry, reducing the speed from more the 6800 m/sec when separate from the launch vehicle, to 17,12 m/sec of speed when it lands.

When: After two attempt the IRDT was launched for the third time on 7 October 2005 at 10:30.

Status: Despise the failed on the inflammation of the second shield, the demonstrator survived and was recovered.

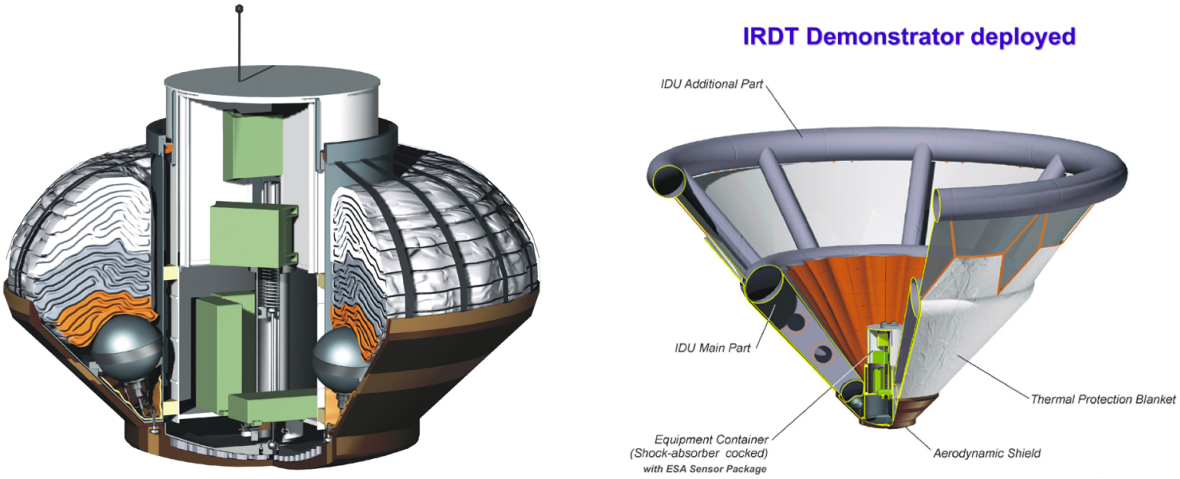

Figure 3.1: a) IRDT; b) IRDT deployed

- Gross mass: 350 kg (770 lb).
- Payload: 250 kg (550 lb).
- Height: 1.83 m (5.99 ft).
- Diameter: 0.52 m (1.70 ft).
- Span: 2.50 m (8.20 ft).

3.2.1.1 IRDT - Involved key technologies

Type of Re-entry Control: After reaching its final altitude the rocket starts to fall rapidly due its weight. The friction with the atmospheric gases during deceleration in the atmosphere causes the shield to heat up and consequently burn. The heating will be more severe the later it will happen during the flight. The reason is that in the lower parts of the atmosphere the density is higher thus the heating is higher. Ideal would be a solution that slows down the capsule while it

is still in the higher parts of the atmosphere. This however can only be reached with very large surface to mass ratios. This requires a very large heat shield relative to the payload. To increase the area of the re-entry capsule an inflatable system is used. During re-entry control is made in two stages. The first one is before the capsule be released, were the spacecraft reoriented on its trajectory. After reaching the maximum altitude the capsule will proceed the descent process in which the first inflammation of the shield occurs. This first shield maintains the traveling velocity ($\tilde{6}$.9 m/sec). The second and last control stage occurs when the capsule is at 14 km altitude. At this point the velocity has already been reduced to 230 km/h. Afterwards this system will guaranty a safe landing.

Type of Capsule: Inflatable

3.2.2 Inflatable Re-entry Vehicle Experiment - IRVE

More than 40 years after the idea of an inflatable re-entry capsule was first published the first successful flight has taken place. Developed by NASA, IRVE became the worlds first successful inflatable re-entry capsule [4]. The aim of the project was to build a new kind of lightweight inflatable spacecraft structure to slow and protect a re-entry capsule during re-entry in the atmosphere at hypersonic speeds.

Purpose: The project was to proof the feasibility to built an inflatable heat shield to slow down and protect itself as it enters the atmosphere at hypersonic speeds. The inflatable acts as an aerodynamic decelerator with a Thermal Protection System (TPS) that guarantee the re-entry survival of the capsule.

Who: NASA

What: IRVE has a mushroom shaped heat shield that is vacuum-packed into a 56 centimeters diameter nose cone. It is launched on a small sounding rocket on Wallops Island, Va.

When: The first launch of IRVE could not be identified in literature. The launch of IRVE-2 took place at 17 August 2009 together with Black Brant-IX 1399lb Payload in Wallops Island (Canada). After considerable upgrades in performance (apogee altitude, the re-entry capsule mass, improvement on the inflatable shield) the IRVE was launched on 23 July 2012.

With considerable upgrades, sInce the apogee altitude, the re-entry capsule mass, improvement on the inflatable on 23 July 2012 the new IRVE-3 was launched.

Status: Currently the next generation of IRVE is under development. Is expected to be launched in spring of 2014 [5].

3.2.2.1 IRVE - Involved key technologies

Type of Re-entry Control: Based on the same concept that the IRDT. After the rocket achieves the celling height it opens inflatable heat shield. The IRVE has a mushroom shape to increase the exposed area and reduce the re-entry process.

Type of Capsule: Inflatable

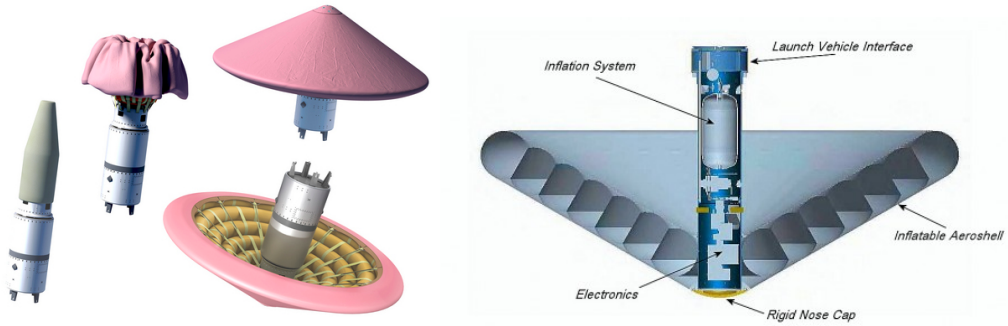

Figure 3.2: a) IRVE deployment; b) IRDT deployed [6]

3.2.3 Hayabusa

Developed by the Japan Aerospace Exploration Agency (JAXA), the Hayabusa project was designed to land, collect and return with a sample from a small near-Earth asteroid named 25143 Itokawa to Earth for further analysis [7].

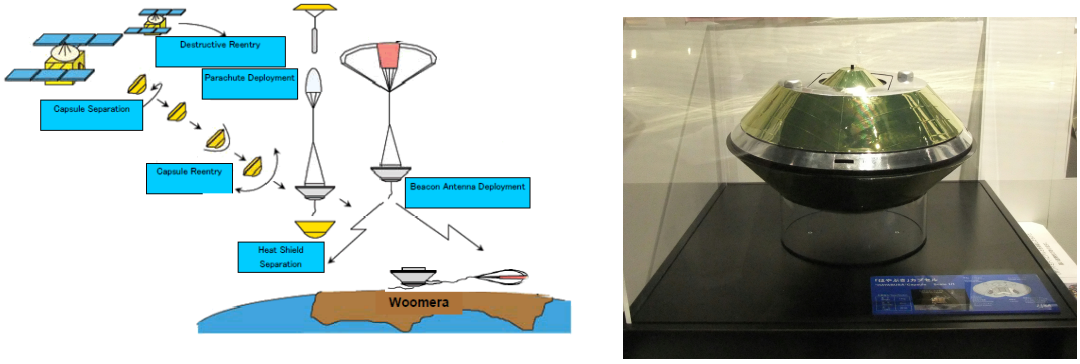

Figure 3.3: a) Hayabusa release[8]; b) Hayabusa Replica [9]

Purpose: The purpose of the Hayabusa probe was to conduct an interplanetary flight and return a sample to the earth. After reaching the designated asteroid with a sample was taken and the returned to earth. Inside the probe was a landing capsule that landed and brought back the collected samples from the asteroid.

Who: The project has developed and executed by the Japan Aerospace Exploration Agency (JAXA).

What: The project contain four main steps: first to independently reach the designated asteroid, second to use a simplified landing device to retrieve a sample, third to autonomously return the probe to earth and fourth to safely land the capsule on ground to allow inspection of the samples. In the context of this mission the re-entry capsule is the most important part. The Hayabusa,

re-entry capsule was made of a heat-shielded with a parachute inside. The parachute was released after the critical descent to slow the capsule down after landing in Australia.

When: Launched 9 May 2003, reentered to the Earth atmosphere on 13 June 2010 in a 20 km by 200 km area, in the Woomera Prohibited Area, South Australia.

Status: Despite being damaged during landing the samples inside the capsule remained intact. The mission was deemed a success.

3.2.3.1 Hayabusa - Involved key technologies

Type of Re-entry Control: The Hayabusa capsule had no active control system; all methods to stabilize were passive. This included a low center of mass and careful selection of the capsule angle of attack during re-entry obtain form the shape of capsule cover by high performance resistant.

Type of Capsule: Rigid.

3.2.4 Young Engineers' Satellite 2 - YES2

One of the most ambitious project, where Delta-Utec SRC and with the ESA Education supervision, challenged students and young engineers all over Europe to design and built a satellite([10] and [11]).

Figure 3.4: a) YES2 contains FLOYD , MASS and Fotino, the spherical re-entry capsule; b) YES2 assembled on FOTON-M spacecraft. [12]

Purpose: The purpose of the mission was to build a low-cost capsule that would return from space to Earth, without the use of any means of propulsion. Instead it was hold and control by a 30 km long and 0.5 mm thin tether, which would lead to a safety land in a pre-determined location.

Who: Build for 450 European students; the project was part of a ESA's and Foton-M3 mission.

What: YES2 is constituted in three components: the Fotino capsule, a Mechanical data Acquisition Support System (MASS) and a Foton Located YES2 Deployer (FLOYD). The Fotino is encased with an ablative material, to protect the scientific equipment and the parachute system inside, as it returns to Earth. At the right moment the Fotino capsule is release from the four straps

that hold it to the MASS. FLOYD is connected with the MASS by a 30 km of 0.5 mm thick tether. Inside of the FLOYD is a robotic spacecraft Foton-M3, which will eject MASS and Fotino towards Earth.

When: Launch on 14 September 2007 in Kazakhstan the YES2 was deployed and release the re-entry capsule on 25 September 2007 to reach Kazakhstan area[13].

Status: Successful

3.2.4.1 YES2 - Involved key technologies

Type of Re-Entry Control: The re-entry will be control for a 30 km long tether.

Type of Capsule: Rigid

3.3 De-orbiting

Reduce space debris, recover information or simply due the technological evaluation are some reasons for the studies on the development of the satellite de-orbiting. Depending on the reason and atmosphere layer that the satellite will be in orbit the approach is different.

Some approaches have been made by a control system with propulsion, but requires a more complex systems to deal with the instability induce by the liquid sloshing of Residual fuel. Other example was presented, in the 2nd IAA Conference on University Satellite Missions and Cube-Sat Workshop, suggesting a control made by a four wing moving independently and thanking advantage of the drag coefficient.

3.4 Re-entry

In order to allowing a larger area for the impact zone, the object needs to respect the limit of 15 J, and the easy way to do it is increasing the ratio between the dimension and weight. That was one of the approaches of the ESA project, IRDT. Where the capsule with a 140 kg makes its first increase of the diameters of 80 cm to 2,3 m and then to 3,8 m.

On May 9th, 2005, the unmanned Hayabusa was launched, to collect and return a sample of a small asteroid. A few months afterwards, near the asteroid, the sample recovery was scheduled. Once the satellite was on the return trajectory the re-entry capsule was released. On June 14th, 2010 the capsule was successfully recovered with the help of a GPS receiver and a rescue team that surrounded an area of 20 Km by 200 km in the South Australia.

NASA launched the Inflatable Re-entry Vehicle Experiment (IRVE-3) to test a space capsule with an inflatable outer shell system. An inflation system pumped nitrogen into the IRVE-3 expanded the inflatable system, increasing the capsule size to about 10 feet diameter. The shell slows and protect hypersonic speed during planetary entry and descent, or as it returns to Earth.

The landing spot was the coast of North Caroline, on Atlantic Ocean.

A similar approach that will be presented in this thesis was developed in the Young Engineers' Satellite 2 (YES2) project. On September 14, 2007, was launched 40 ESA experiment with a

mission to experiment a 12 days in orbit of zero gravity. One of the experiments was the YES2, a 36 kg student-built project that was deployed September 25, 2007 with objective to release a small spherical re-entry capsule and reach the Kazakhstan. The final mission experiment did succeed and even establish a world record for the longest artificial structure in space, but any signal was received form the capsule after the re-entry and it was never been recovered, meanly calculation indicates the Aral Sea has the landing area.

Chapter 4

De-orbiting Control

The satellite trajectory is described by its orbital parameters. In an ideal situation without disturbances the orbit would prevail infinitely. However in reality the satellite is affected by a number of disturbances of which in low earth orbit the atmospheric friction is the most severe. This friction can be reinforced by changing the attitude generating trajectory relative to the initial trajectory has a faster altitude decrease rate. There are a number of conditions that influence the trajectory. The two main factors are: vertical density profile of the atmosphere and resulting drag force. In the following figure the effect is presented:

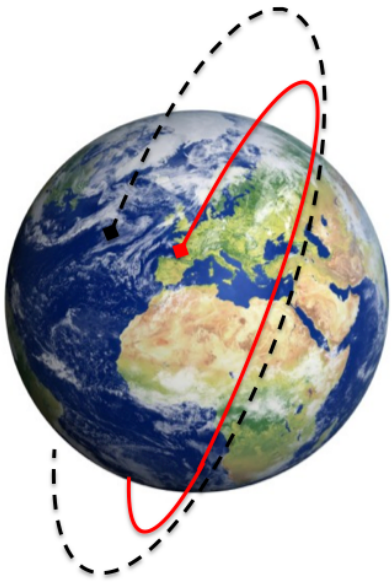

Figure 4.1: Drag force effect on the trajectory. Lower drag force overshoot the landing (black). Higher drag force, faster de-orbiting (red)

For any satellite on a space mission is very important to study the drag and atmospheric condition. This is done to reduce the influence in the trajectory. Since the GAMASAT does not carry a propulsion system the possibilities of influencing its trajectory using the state of the art are limited.

In order to allow the new method of differential drag to be working it is required to autonomously calculate the satellites decent during de-orbiting. Its one of the aims of this study to to understand the influences on the satellite trajectory and to use this knowledge to influence the location and trajectory of the satellite up to the moment of the releasing the capsule. The findings of this study will be presented in the following sections of this document.

4.1 Atmosphere - Vertical Structure

The atmosphere vertical structure is described by the following parameters: air density, temperature, pressure and molecular mass. The distribution of each parameter can been seen in the following figure:

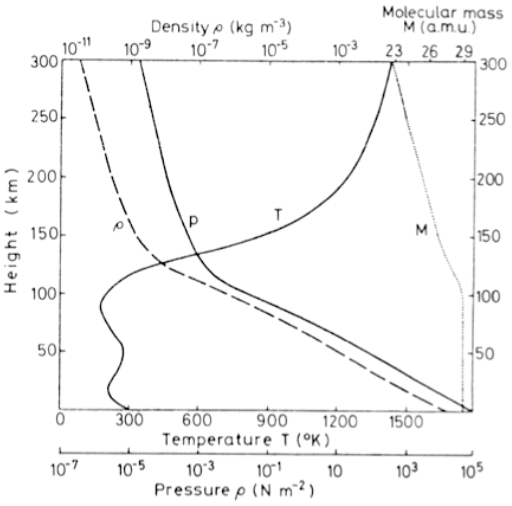

Figure 4.2: Atmosphere Vertical structure

The density of Earth's atmosphere is a combination of the pressure and molecular mass. The atmosphere is constituted of gases that surround our planet.

These gases consists of a combination of numerous atoms and molecules. The number of atmospheric particles or the molecular mass decreases with altitude, decreasing the pressure leading to a decreasing of the air density. This can be described using to relation between pressure and density. In approximation the atmosphere density can be described by the model of the ideal gas. It relates between relate density ρ, pressure P and temperature T:

$$\rho = \frac{RT}{PM_{mol}} \tag{4.1}$$

with R being the gas constant (8,31 J $K^{-1}mol^{-1}$) and M_{mol} is the molecular weight of the gas.

The four parameters are connected by the formula above 4.1. By solving the equation the density can be described it as a function of pressure and temperature. The temperature has to be analyzed in more detail as it not only depends on the gases but on other external factors. These factors will be described later in this document.

4.1.1 Density

The atmosphere is in equilibrium of gases that are constantly flowing upward by the internal pressure and being forced downward by the gravity. This keeps the atmosphere in a hydrostatic balance. The pressure is higher with lower altitude. This effect can be experienced by everyone who has already climbed a mountain. The reason for this effect is that with every meter gained above ground the mass above oneself is smaller thus is the pressure.

Analyzing the pressure variation in an infinitesimally way, as shown in the figure below, comes the following equations:

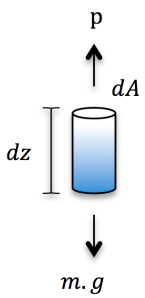

Figure 4.3: Pressure vs gravity

$$P = - \frac{m.g}{dA} \tag{4.2}$$

for the mass we have:

$$m = \rho.V \tag{4.3}$$

and the volume comes as:

$$V = dA.dz \tag{4.4}$$

leading us to:

$$P = - \rho.g.dz \tag{4.5}$$

The expression above indicates the pressure, not taking in to consideration gravity or/and density variation which is true in the Earth surface, but it becomes incomplete for the atmospheric pressure evaluation. Therefore for a valid atmospheric pressure expression and it variation, we need to consider a density and gravity variation with altitude:

$$\frac{dP}{dz} = - \ \rho(z) \ \ g(z) \tag{4.6}$$

The atmospheric pressure is approximately given by:

$$P = \ \ p_0.e^{-\frac{g(z).M_{mo}(z) \ \ h}{R \ \ T(z)}} \tag{4.7}$$

Being the pressure scale height, H defined by:

$$H(z) = \ \ \frac{R \ \ T(z)}{g(z) \ \ M_{mol}(z)} \tag{4.8}$$

Relating the equation 4.7 and 4.8 comes:

$$P = \ \ p_0.e^{-\frac{h}{H(z)}} \tag{4.9}$$

The variation of density with height can be derived similarly, resulting in:

$$\rho = \ \ \rho_0.e^{-\frac{h}{H(z)}} \tag{4.10}$$

This equation it is only valid where the temperature remain constant with height in a vertical structure. This is the case of the thermosphere which is the layer of interest for this study. This invariability lead us to a density scale height equals to the pressure scale height. If this would not be the case we would otherwise need to consider that variation of the temperature in the calculation of the density scale height.

Comparing equations 4.9 and 4.10 we see that there is a similarity, which was expected from the analysis of Figure 4.2. However since temperature shows a variation that is almost equal to the gain of the density over the pressure the effects of temperature needs further analysis.

4.1.2 Temperature

A more detailed way to describe the temperature variation can be achieved by atmospheric models. In this document, as shown in Figure 4.4, a NRLMSISE- 00 model was used. This model

takes the temperature variation 400 km over Delft, in the Netherlands in to account . It shows the density variations over a solar flux cycle, between 2000 and 2006.

This section will present a brief review about the impact of temperature in the atmosphere dynamics and consequently in the air density.

For the purpose of this thesis only the variation until 200 km will be analyzed.

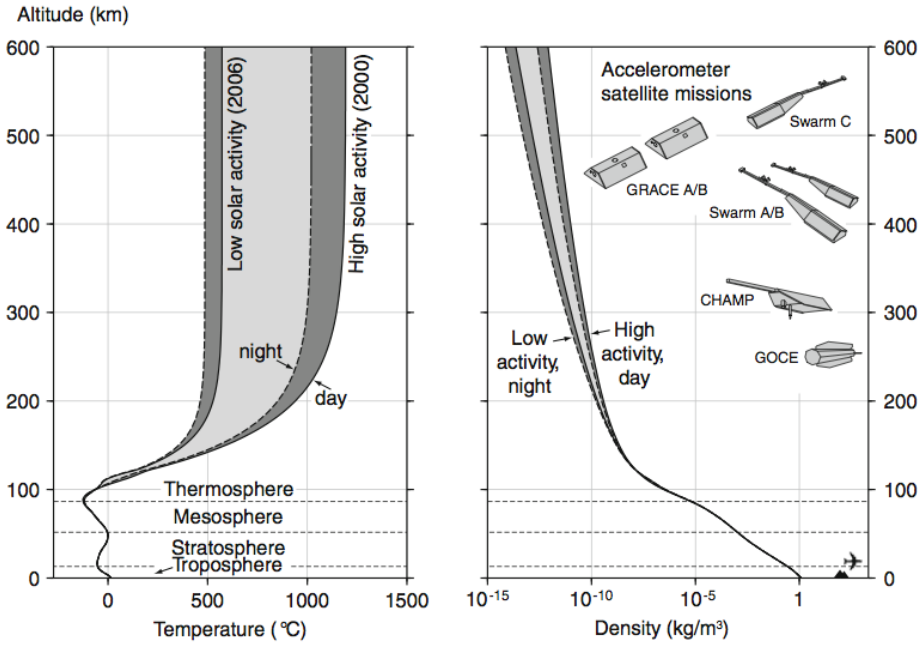

Figure 4.4: Density variation and temperature with altitude, according to the NRLMSISE-00 model [14]

Temperature is a measure the thermal energy of a particle due to micro vibrations. These vibrations increases the chances of collision between particles and objects consequently increases the temperature of these objects.

In the atmosphere the Sun is responsible for the increase of the ambient temperature. Although the atmosphere temperature reaches more than $1000\,^{\circ}C$ in the thermosphere collisions are scarce due to the lower density, making the thermosphere bearable.

By the ideal gas law the temperature T is given:

$$T = \frac{P\ V}{n\ R} \tag{4.11}$$

with P being the pressure, V the volume, n the number of moles and R the universal gas constant.

4.1.2.1 Overview

The Sun energy is the source for the ambient temperature. The energy flux of the sun can be approximated as a black body source with 5800 K [23]. According to the Planck law it transmits energy from low energy radio waves to high energy X-ray.

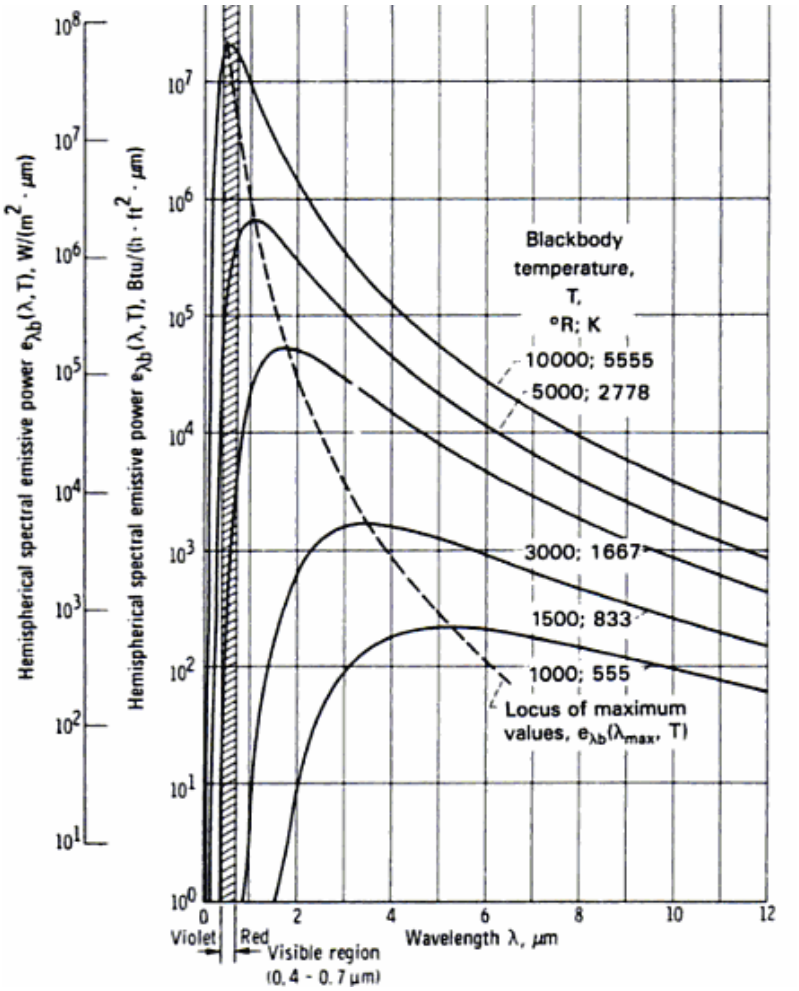

Figure 4.5: Black body Curves [18]

As it can be seen the peak of the sun activity is at 500 nm [23]. The level of radiation that reaches the earth and its atmosphere is dependent on a number of factors. These factors will be described in the following sections. It reaches the atmosphere through ultraviolet radiation and X-radiation, heating and ionizing the atmospheric gases.

The levels of radiation change with latitude and longitude and decrease the distance from the Sun and change with the amount of solar activity.

Temporal Variation:

Temporal variations include diurnal variations, seasonal cycles and long periods. These variations directly influence the change of electron density. Diurnal variations are caused by changes of solar radiation, which disappear at night.

The seasons also influence the variation of the electron density due to the change of the zenith angle of the sun and the intensity of the flow of ionization. In equinox, the effects of the ionosphere are larger, whereas in solstice, the effects are minor.

Location:

The geographical location also influences the variation of electron density, because the overall structure of the thermosphere it is not homogeneous. It changes with latitude, due to the variation of the zenith angle of the Sun, which influences directly the level of radiation, which changes, in turn, the electron density in the ionosphere. The influence of longitude, due to the non-coincidence of the magnetic and geographic poles, is sensitive only in the higher regions.

Solar activity:

The sun magnetic activity varies cyclically in periods of approximately 11 years.

These activities are associated with occurrences of sunspots, and the increase of ionization is proportional to the number of spots. The period of maximum solar activity caused an increase in the number of sunspots and consequently, the number of electrons present.

At the core of the Sun with high temperatures, density and pressure does the process of nuclear fusion of hydrogen into helium. The energy that is generated in the core is transported by radiation to a radiative layer that surrounds the core. Between the radiative layer and the next layer it as an interface were the sun's magnetic field is generated. The next layer is the convection zone were power transmission is by convection, transporting the less dense material to the Sun's surface. The last layer, corona layer consist of plasma. The high temperature ionized gases that escape through coronal holes, creating the Solar Wind that is responsible for the geomagnetic storms. The geomagnetic field controls of the ionized gases movement, so the geomagnetic storms will dramatically change it motion and consequently will affect the density. Higher the geomagnetic storms, higher will be the air density.

Equation 4.11 show that by increasing the temperature and for a same volume, the pressure will consequently increase. Taking that conclusion to the equation 4.1 it is obvious that the air density will decrease.

In case of increasing the temperature in same pressure the gases will rise. Followed by the equation 4.3 the density will consequently increase.

Greenhouse effect:

The temperature n stable state of any object in an orbit around sun depend on a number of factors. The main factors have been described earlier. There is however another factor that is resulting from the atmosphere itself. For an spherical body in earth orbit the temperature would only be dependent on its color, hence the amount of absorbed to emitted heat. This is shown by the Wien's displacement law[15]:

$$\lambda_{max}(nm) = \frac{2.897(8)10^6(nm)}{T(K)} \tag{4.12}$$

The amount of radiation absorbed depends on the reflectivity of the planet, designated of Albedo (Al) and the Solar constant of the planet governed by the equation:

$$Powerabsorbed = \frac{AreaSolar(1-Al)}{(distance)^2} \tag{4.13}$$

In case of emitted radiation the equation that describe it is the Stefan Boltzmann law:

$$\frac{Power}{Area} = \sigma T^4 \tag{4.14}$$

Another difference between the Power emitted and absorbed is the Area. Assuming a uniform temperature all around the world, the emitted power is made all around the surface of the planet, so the Area will be $4\pi R^2$. In case of absorbed radiation, only the area that is faced to the Sun is absorbing, there so the Area is πR^2.

Equating these two equation 4.13 and 4.14 the equilibrium temperature can be calculated as a result of incoming and outgoing fluxes.

$$\begin{aligned}(\pi R^2)Solar(1-Al) &= (4\pi R^2)\sigma T^4 \\ T &= \sqrt[4]{\frac{Solar(1-Al)}{4\sigma}}\end{aligned} \tag{4.15}$$

$$\begin{aligned}Solar_{Earth} &= 1370W/m^2[16] \\ A_{Earth} &\approx 0.31[17]\end{aligned}$$

Based on these factors it can be calculated that the average temperature of earth without any further effect would be ≈255 K ($-18\,^\circ C$). Since the actual measured average temperature of earth is actually in the range of ≈288K ($+15\,^\circ C$) this indicates another influence factor. This factor is the green house effect of atmosphere. While the man made green house effect has been matter of discussion in the recent years it is an often overlooked fact that without the natural green house

effect earth would not be habitable. Since the extension of the atmosphere is directly influenced by earth surface temperature a further look is taken onto it.

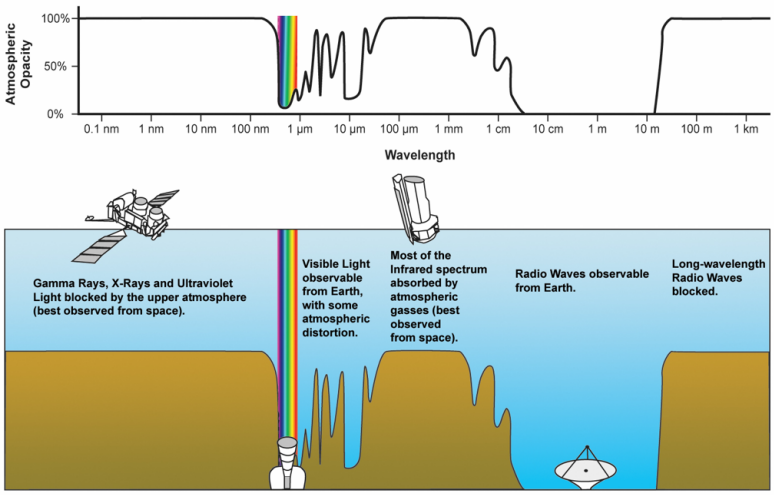

Figure 4.6: Earth transparency of atmosphere [24]

Due to the fact that the atmosphere is largely transparent for high energetic visible light but not transparent to thermal parts 4.6 of the spectrum that means that on the one hand the energy of the sun can enter the atmosphere on the other the peak of the earth own black body radiation (at 250 K) is in thermal infrared an cannot pass. The source of this natural green house effect is largely the water vapor in the atmosphere. In the recent years additional man made effects, largely CO2, by burning of carbon based energy sources has been introduced to the atmosphere. This further reduces the transparency of the atmosphere. With regard to the focus of this study this has two effects. First the temperature of the lower atmosphere rises due to the inability of thermal radiation (heat) leaving the atmosphere. Secondly due to the reduced transmission the outer layers of atmosphere actually cool down in absence of this heat flux. Thus in contrary to popular believe the atmosphere shrinks and friction decreases. This factor is influencing the time frame of how long a satellite can maintain orbit and its de-orbit. However for the purpose of the study this effect can be considered static.

4.1.2.2 Simplified Model

After describing the properties of the atmosphere it becomes apparent that these values cannot be measured during the re-entry process. For simulation purpose a simplify exponential density model of the atmosphere is enough to describe the satellite dynamics. Therefore the following table is used on the density estimation:

Following the table form Figure 4.7 the density is calculated for each layer using the equation 4.10. Where the base altitude, h_0, nominal density, ρ_0, and scale height, H, can be taken from column 2^{nd}, 3^{rd} and 4^{th} column respectively.

Altitude h_{ellp} (km)	Base Altitude h_o (km)	Nominal Density ρ_o (kg/m^3)	Scale Height H (km)	Altitude h_{ellp} (km)	Base Altitude h_o (km)	Nominal Density ρ_o (kg/m^3)	Scale Height H (km)
0–25	0	1.225	7.249	150–180	150	2.070×10^{-9}	22.523
25–30	25	3.899×10^{-2}	6.349	180–200	180	5.464×10^{-10}	29.740
30–40	30	1.774×10^{-2}	6.682	200–250	200	2.789×10^{-10}	37.105
40–50	40	3.972×10^{-3}	7.554	250–300	250	7.248×10^{-11}	45.546
50–60	50	1.057×10^{-3}	8.382	300–350	300	2.418×10^{-11}	53.628
60–70	60	3.206×10^{-4}	7.714	350–400	350	9.518×10^{-12}	53.298
70–80	70	8.770×10^{-5}	6.549	400–450	400	3.725×10^{-12}	58.515
80–90	80	1.905×10^{-5}	5.799	450–500	450	1.585×10^{-12}	60.828
90–100	90	3.396×10^{-6}	5.382	500–600	500	6.967×10^{-13}	63.822
100–110	100	5.297×10^{-7}	5.877	600–700	600	1.454×10^{-13}	71.835
110–120	110	9.661×10^{-8}	7.263	700–800	700	3.614×10^{-14}	88.667
120–130	120	2.438×10^{-8}	9.473	800–900	800	1.170×10^{-14}	124.64
130–140	130	8.484×10^{-9}	12.636	900–1000	900	5.245×10^{-15}	181.05
140–150	140	3.845×10^{-9}	16.149	1000–	1000	3.019×10^{-15}	268.00

Figure 4.7: Exponential Atmospheric Model [19]

4.2 Drag Force vs attitude

The drag force is the force that opposites the movement of a body on a fluid and it is given by the following expression:

$$F_D = \frac{1}{2}\rho CxAv^2 \tag{4.16}$$

The equation quantifies the force imposed to an object with an area A and velocity v and a coefficient of aerodynamics $\boldsymbol{Cx}$, that crosses a fluid with density ρ.

By the drag force equation it is clear that during the body trajectory only the exposed area and velocity can be controlled, and by decreasing the exposed area or the velocity the drag force decreases.

This relation can be seen in sports as racing sport, ski, horse racing, cars or in the fighter aircrafts by retracting the exposed area of the object/runner to the wind so it can decreases the drag force by reducing the exposed area and increases the speed.

We can also see that the amount of drag force suffered by an object depends on drag coefficient Cx that describes the object aerodynamics.

4.2.1 Drag Coefficient

The drag coefficient ***Cx*** describe a relationship between the drag force, density, exposed area and velocity that depends only on the object shape. However, since the fluid behavior depends on density and even on velocity different coefficients apply for different conditions. For example, at, higher density (such as at MSL density) the flow of around a object impose modifications to the interaction between air particles, cause such flow to be smooth around the object and causing turbulence at the wake region. As showed in figure 4.11.

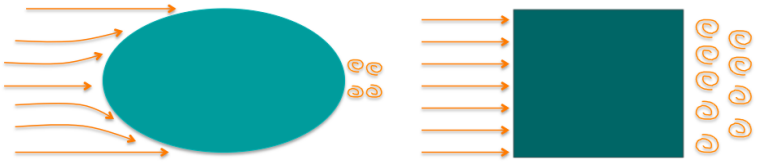

Figure 4.8: Flow through a Sphere vs Cube

In very low density situations, such as in the thermosphere, particles are so scarce that interaction between particles are negligible; therefore the derivation of the drag coefficient in such conditions can be performed by addressing the single interaction of the particles with the exposed are of the object.

4.2.2 GAMASAT Drag Coefficient

As seen previously the higher the altitude the lower the number of particles will be. The number of particle is so low that it trajectory is not affect by each other and so the drag coefficient will be higher.

Unfortunately the exact flow condition that the satellite will be facing within the outer parts of the atmosphere is unknown. To find the approximate value an analysis of the linear momentum and the kinetic energy of possible collision types was made. The type of collision is described by the particles attitude. In a first step the particle attitude is described by the conservation of momentum. Initially a particle, m, with velocity v impact in a satellite, M, at rest, $V = 0$, as showed in the Figure 4.9. After the collision the particle have a new velocity, v', and the satellite remains at rest.

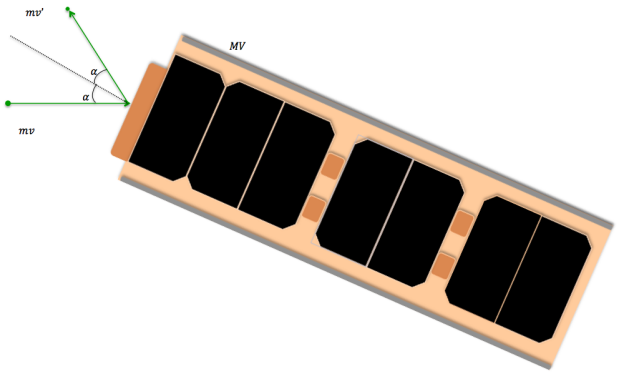

Figure 4.9: Kinetic Energy transfer due the collision

With the conservation momentum and the figure we can take the following equation :

$$m\Delta v = M\Delta V$$
$$m(v+v') = M\Delta V \tag{4.17}$$

$$m = \rho A v \Delta t$$
$$\rho A v \Delta t (v+v') = M\Delta V$$

$$\rho A v (v+v') = M\frac{\Delta V}{\Delta t} \tag{4.18}$$
$$\rho A v (v+v') = Ma$$
$$F_D = \rho A v (v+v')$$

Considering that k is the relationship between the particle velocity before v and after v' the collision.

$$v' = kv \tag{4.19}$$

$$F_D = \rho A v^2 (1+k) \tag{4.20}$$

Relating the Equations 4.16 and 4.20 we have:

$$\rho A v^2 (1+k) = \frac{1}{2}\rho C x A v^2 \tag{4.21}$$

$$\frac{1}{2}Cx = 1+k$$

$$Cx = 2(1+k) \tag{4.22}$$

It is expected low, α angles between the particle and the satellite. The types of collision can be analyzed according to the particle state after the collision. They can be:

- Perfectly inelastic collision;
- Perfectly elastic and specular collision;
- Non-elastic collision.

4.2.2.1 Perfectly Inelastic Collision

The inelastic collision describes the absence of velocity after the collision, so the kinetic energy is not conserved. In this case the particles get stuck in the object surface. This leads to an accumulation of particle in the object surface (e.g. the case of bugs that get stuck in a car window). So physically what happens is:

- velocity before the collision v = v;
- velocity after the collision v' = 0;

Taking to the equation 4.19 we have a $\boldsymbol{k} = 0$;
Replacing in the equation 4.25 leads to a minimum of $\boldsymbol{Cx} = 2$.

4.2.2.2 Perfectly elastic and specular collision

In a case of complete elastic and specular collision the particles are projected with the same angle that collided with the object surface as the initial trajectory, but in the opposite direction. So the drag coefficient is given by:
velocity after the collision $v' = v.cos(2\alpha)$ substituting in the equation 4.25 we have:

$$v' = v.cos(2\alpha) \tag{4.23}$$
$$k = cos(2\alpha) \tag{4.24}$$
$$Cx = 2[1+cos(2\alpha)] \tag{4.25}$$

Taking an $\alpha = 0$, lead us to a maximum of $\boldsymbol{Cx} = 4$.

4.2.2.3 Non-elastic collision

In case of a non elastic collision, after the collision the particle is projected with a different energy. In this case the approach is to analyze the conservation of kinetic energy, that is given by

the equation bellow:

$$\frac{1}{2}m(v)^2 = \frac{1}{2}m(v')^2 + \frac{1}{2}M(\Delta V)^2 \tag{4.26}$$

Comparing equations 4.17 and 4.26 we can see that the kinetic energy corresponds of the moment of inertia multiply by $\frac{1}{2}$ the velocity. In case of the satellite the momentum is already low due to the low variation of velocity before and after the collision, so by multiplying by $\frac{1}{2}$ ΔV the kinetic energy variation of satellite is negligible compared with that of the particle.

After the collision the particle is deviated from the trajectory with a different velocity, which relates to the initial velocity according to :

$$\frac{1}{2}mv^2 = e\frac{1}{2}mv'^2 \tag{4.27}$$

$$\begin{aligned} v &= \sqrt{e}v' \\ \varepsilon &= \sqrt{e} \end{aligned} \tag{4.28}$$

The difference between velocity before and after the collision, the k of equation 4.19, is affected by the coefficient of elasticity or restitution ε . The ε parameterizes the energy that dissipates during the collision. The coefficient of elasticity is limited between $0 < \varepsilon < 1$, limited by a perfectly inelastic collision and elastic collisions, respectively. For typical a non-elastic collision we will have an $\varepsilon = 0,3$ [20].

Therefore an analysis for a specular and non-specular collision is needed.

Non-elastic collision and Specular collision

In specular collisions the k is given by the equation 4.24 multiplied by the coefficient of elasticity $\varepsilon = 0.3$. There come that:

$$\begin{aligned} k &= \varepsilon cos(2\alpha) \\ Cx &= 2[1 + \varepsilon cos(2\alpha)] \end{aligned} \tag{4.29}$$

$$\tag{4.30}$$

For an $\alpha = 0$ we have:

$$Cx_{max} = 2[1 + 0,3(1)] \tag{4.31}$$

$$Cx_{max} = 2,6 \tag{4.32}$$

$$\tag{4.33}$$

Non-elastic collision and Non-Specular collision

In case of a non-specular collision the particle can take any angle β, as showend in figure 4.10, with the surface after the collision limited by the object surface. Leading a given k' of:

$$k' = cos(\alpha + \beta) \tag{4.34}$$

When collising with the GAMASAT surface the particles are deflected along any angle $\beta \in [-\frac{\pi}{2}; \frac{\pi}{2}]$ according to a probability density function given by the possible model:

$$P(\beta) = \frac{1}{2} cos(\beta) \tag{4.35}$$

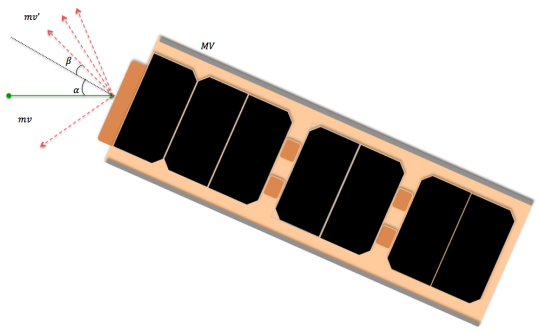

Figure 4.10: Non-specular collision

So the new k is given:

$$k = \int_{-\pi/2}^{\pi/2} \frac{1}{2} cos(\alpha + \beta) cos(\beta) d\beta \tag{4.36}$$

(*Details can be found in Appendix A.6*)

$$k = \int_{-\pi/2}^{\pi/2} \frac{1}{2} [\frac{1}{2} cos(\alpha + 2\beta) + cos(\alpha)] d\beta$$

$$k = \int_{-\pi/2}^{\pi/2} \frac{1}{4} [cos(\alpha + 2\beta) + cos(\alpha)] d\beta \tag{4.37}$$

$$k = \int_{-\pi/2}^{\pi/2} \frac{1}{2} [\underbrace{\frac{1}{2} cos(\alpha + 2\beta)}_{= 0 \text{ (A.8)}} + \frac{1}{2} cos(\alpha)] d\beta$$

Therefore k is given:

$$k = \frac{\pi}{4} cos(\alpha) \tag{4.38}$$

In this case we have:

$$Cx = 2(1 + \varepsilon[\frac{\pi}{4} cos(\alpha)]) \tag{4.39}$$

$$Cx_{max} = 2[1 + 0.3(\frac{\pi}{4})]$$

$$Cx_{max} \approx 2.47 \tag{4.40}$$

4.2.3 GAMASAT Drag Force

It is expected that both collisions specular and non- specular occur, so a weighted arithmetic average between 4.32 and 4.40, has been made to estimate the drag coefficient.

$$Cx = 0,5(2,47) + 0,5(2,6)$$

$$Cx \approx 2,54 \tag{4.41}$$

From there the resulting drag force can be calculated. As explained earlier the GAMASAT is a 3U CubeSat. That gives a ratio between the smaller cross section and the larger one, a drag force of 1: 3; accordingly the drag force of these two section as also a ration of 1:3. Therefore the the projected landing area can be redefined by switching between the two cross sections. By controlling the actuation time of the two states, will take us to a better altitude for the capsule release.

The proposed process works as follows. In a first step the orbit position, velocity and time are measured using a GPS receiver. This position value is then used to update the predictions for the landing area. Depending on whether the landing area is undercut or overshoot by the satellite an update is made in the relative duration of cross section exposure time of the satellite. The time between two measurements is 30 minutes thus is the resulting cycle time. Switching between the two cross section is performed by rotating the space craft by 90°.

4.3 Re-entry forecast

The re-entry forecast is essential to correctly apply the control strategy.

The main purpose of the algorithm is to optimize the time for the exposure of the larger cross section of GAMASAT. The estimation and optimization is based on an simplified model that predicts the landing point.

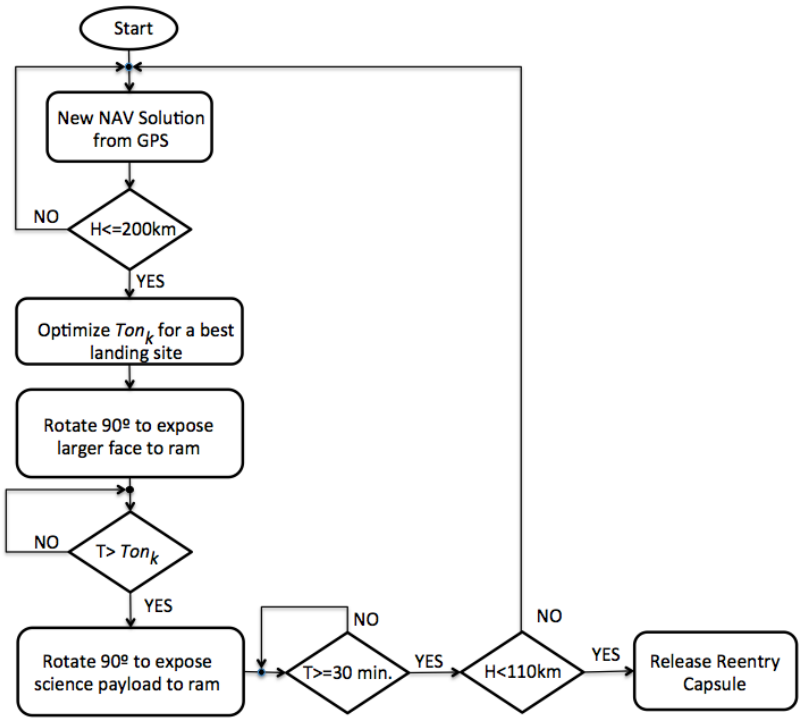

Figure 4.11: Flowchart of De-orbitng Control Algorithm

4.3.1 Time of Control

At the beginning of each cycle GPS readings are taken. Based on the new navigation data the the algorithm calculates the number of orbits until reach the release zone. The release area is the point in the orbit from which the capsule will reach the desired landing area with further steering operations.

With the purpose of reduce the difference between the satellite position and the release area, a time T_{on} for the larger exposed area is calculated. The differential drag will work with two states. A small and a big surface area. The difference between those is a factor of three. By exposing the larger surface the satellite is decelerated thus its overall energy is decreased (sum of the potential and kinetic energy). Therefore with this method the satellite will fall faster to the ground. However by decelerating the satellite will go to a lower orbit which in contrast will increase its orbital velocity. Hence relative to the release area the satellite will overshoot. This results in a seemingly paradoxical situation that decelerating the satellite will make it catch up with the release area and accelerating thereby increasing the orbit and decreasing the velocity will make it fall back. Keeping this in mind the algorithm calculates the T_{on} time. That means the time in each 30 minutes control interval which exposes the larger surface area.

In order to have the maximum capacity to act on the crash site, the ideal is that the average value of the control is at mid scale. In accordance to this a T_{on} with a duty cycle of 50%.

However, this would correspond to quite wasting life of the satellite and wasting time with the scientific payload pointed to the apparent wind. Thus, we use the value of 25% as an average between the optimal value in terms of acting ability (50%) and the optimal value in terms of performance of the satellite (0%).

4.3.1.1 Optimize Time of Control

The algorithm computes the T_{on} time for the current cycle between 0 and 25 minutes. This calculation is based on the new landing area and based on he assumption that on the next cycle T_{on} will used 25% of the 30 minutes cycle.

Previous simulation showed that would take $\approx$ 5 seconds for the algorithm calculate the T_{on}. However a less capable microprocessor is expected to be use, increasing the time for the calculus. Assuming that the microprocessor will be 100 times worst the first 5 minutes will be for the calculation.

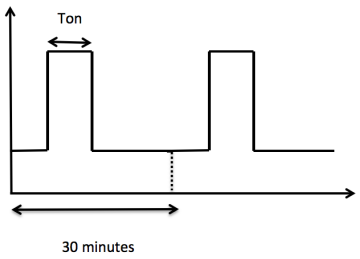

Figure 4.12: De-orbiting Control cycles

4.3.2 De-orbiting Control phase

The de-orbit control phase is the time during the re-entry phase in which the satellite actively alters its descent path in order to land in the desired landing zone. This is done using the differential drag method. As explained earlier this control takes place between 200 and 110 km orbit height. In the following the control mechanisms will be explained in detail.

Analyzing the orbit properties shows that the higher the orbit the more control cycles can be done. However analysis also shows that due to higher inherent uncertainties above 200 km there is no point in performing de-orbiting control above such altitude. This means that even if the satellite is correctly actuated the remaining errors will not allow to guarantee the landing in the predicted area. This is shown in Figure 4.13. On the other hand for orbits below 110 km there is only very little time left as the satellite will de-orbit within a few minutes. Thus the actuation is too limited and landing region variability will result in an error of 50 km cross-track and 500 km along track.

Therefore for a efficient control, the actuation needs to be performed between the 200 and 110 Km.

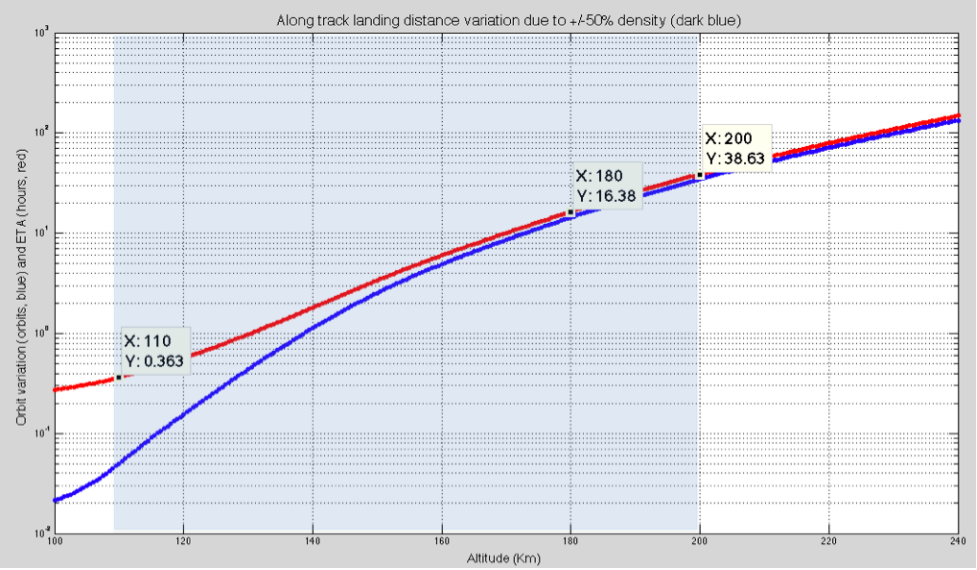

Figure 4.13: Orbit vs Altitude (red - density without variability) (blue - density with +/- 50% of variability)

Actuation will occur in cycles of 30 minutes, each cycle initiating with a new GPS reading. For energy consumption management, the onboard GPS receiver will be operated sporadically, having been determined that 30 minutes intervals between observations is adequate to maintain a suitable ephemeris [21].

In each cycle, the satellite will rotate 90° to expose one of its larger faces to the apparent wind, maintain that attitude for a time interval of T_{on} minutes and return back to the normal attitude (smaller face aligned with the apparent wind). This rotation will increase the exposed area 3 times, decreasing its ability to overcome air resistance, designated as ballistic coefficient of the satellite. Adjusting the duty cycle T_{on} against the duration of the cycle allows to actively control the re-entry location. In order to perform such rotation in a short amount of time (few seconds), specific reaction wheels will be employed. These will have significant actuation effectiveness, but low accuracy, since upon rotation the ADCS will perform any required fine-tuning.

4.3.3 Control Strategy

This is necessary as the conditions influence the state of the capsule and shall therefore be included in the simulations. The algorithm that is used to estimate the time for the larger cross section considers three main guidelines :

- At cycles of 30 minutes new NAV solution are given by the GPS and so, at each cycles new T_{on} will be calculate;
- The T_{onk} is estimated that for in the next interaction the $T_{on(k+1)} = 25\%$ of 30 minutes;

- The capsule will be released at 110 km of altitude.

4.3.4 Release of Capsule

When the satellite reaches the altitude of 110 km the control is stopped. From there on only the capsule specifications are used until it reaches the Earth surface.

4.4 Simulation

From the chapter 4.1 (Vertical Profile of the atmosphere) the relevant formulas to describe the state of the environment has been described. In chapter 4.2 (Drag Force vs attitude) formulas describing the resulting drag of the satellite and later the capsule have been identified. Figure 4.14 shows the overall scenario and the parameters.

Since these equations are very difficult or impossible to solve by analytical means a numerical solver is used. In the following sections this solver is described in detail. Based on the influence parameters the different interdependencies were identified. The resulting block diagram can be seen below:

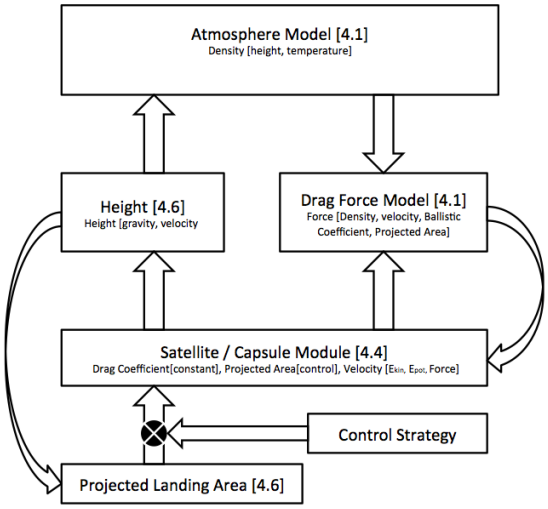

Figure 4.14: Block Diagram

4.4.1 Runge-Kutta method - Overview

Runge-Kutta method is a numerical analysis, to solve ordinary differential equations. For a given initial condition 4.42 and a function that describe how a variable changes relatively to another variable, Equation 4.43 the Runge-Kutta solve it giving the new conditions, by recurrence

the initial conditions and the step.

$$Initial\ conditions: Y = Y_0; \tag{4.42}$$

$$\frac{dY}{dt} = f(t,Y) \tag{4.43}$$

Due the good compromise in calculation speed and accuracy the 4^{th}order of Runge-Kutta method is used to estimated the satellite trajectory.

Matlab was used in this thesis to create the mathematical solution. It was chosen as it already offers a number of potential solvers as the Runge-Kutta method that can be find as ode45, with the following initial parameters:

[t,x] = ode45(@fname, tspan, xinit, options)
with a given parameters:

- fname - is the name of the M-file function used that gives the integrals corresponding to the state variable;
- tspan is the vector with the time limits of integration and the time steps;
- xinit is the vector of initial conditions.
- options offers further parameters to refine the function. Information can be found in the help session of MATLAB. For the purpose of this study the default value is sufficient.

For the output we have:

- t is the value of the independent variable at which the solution array x is calculated.
- x is an array (or matrix) with size length(t) by length(xinit). Each column of x is a different dependent variable.

4.4.2 GAMASAT parameters

In case of the estimation of GAMASAT trajectory the function ode45 receives the following parameters:

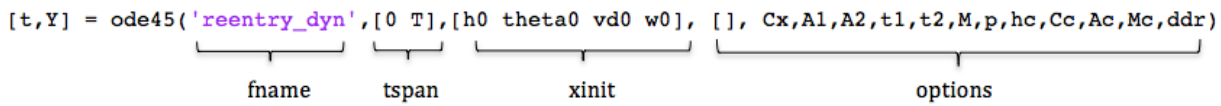

Stranding from the end we have.

options: The options will be specified for GAMASAT and capsule parameters in tables 4.1 and 4.2. These parameters are used for the de-orbit control and described the trajectory.

4.4.2.1 GAMASAT specifications:

Satellite Specifications	
Small cross section (A1)	0.01 (m^2)
Larger cross section (A2)	0.03 (m^2)
Weight (M)	3.0 (kg)
Duty cycle (p)	25 (%)
Time of exposure for A1 (t_2)	30*60 (sec)
Time of exposure for A2 (t_1)	[2*60 25*30] (sec)
Drag coefficient (C_x)	2,54
Density variability (dd)	50 (%)

Table 4.1: GAMASAT Specifications

Capsule Specifications	
Release altitude (h_C)	$110 * 10^3 (m)$
Wind exposed area (A_C)	$\pi * 0.045^2$ (m^2)
Capsule weight (M_C)	0.15 (kg)
Drag coefficient (Cc_x)	0.9

Table 4.2: Re-entry Capsule Specifications

xint: The initial conditions gives the satellite displacement, Table 4.3:

Initial Conditions	
Altitude of actuation (h_0)	$200\,10^3 (m)$
Angle position (θ_0)	$2pi[0:1](rad)$
Descent velocity (vd)	$0(m/sec)$
Angular velocity (ω_0)	$\sqrt{\frac{9.8}{6350000+h0}} * \frac{6350000}{6350000+h0} (rad/sec)$

Table 4.3: Start conditions for the de-orbiting control

tspan: - The iteration time of it will be the 30 minutes cycle [0 t_2]

fname: The ode45 uses the **re-entry_dyn** function to integrated the variables of state and the satellite specification. In each iteration the function gives the new information based on velocity, acceleration and the air density.

Since the state and fluctuation of air density are unknown and cannot be measured during the mission, the author assumes an exponential atmospheric model as starting point for the calculation. The atmospheric values are shown in Figure 4.7. This can only be an approximation and thereby the control phases will allow to correct errors by increasing or decreasing the T_{on}.

Function for the dynamics description

To get the new satellite location the function will determine the satellite velocity (linear and angular) and the accelerations (normal and tangential). The velocities are given by integral of the altitude and angular position. To get the acceleration some analyses are needed.

The movement of the Earth and the satellite movement relatively to the Earth will lead us to an analyses with non inertial referential and inertial referential.

To get the satellite acceleration will be analyze the Coriolis effect.

When we describe an object movement, velocity and acceleration, we are doing relatively to a referential frame. In our case the object is the satellite and the referential is the Earth. So the description of satellite movement will be made with two referentials: a non inertial and an inertial reference. The non inertial is the relation between a vector, $\vec{R_{NI}}$, and one point of the Earth to the satellite, where this point is rotating with an angular velocity of ω_{Earth}.

Since not only the Earth is rotating, but also the satellite relatively to the Earth, the inertial reference is basically the relation between vector, $\vec{R_I}$, the satellite rotation relatively to the Earth, from a outsider Earth perspective, as the Earth is fixated. There so the velocity is given by:

$$\dot{\vec{R_I}} = \dot{\vec{R_{NI}}} + \vec{\omega} x \vec{R} \quad [22] \tag{4.44}$$

$$\ddot{\vec{R_I}} = \ddot{\vec{R_{NI}}} + \dot{\vec{\omega}} x \vec{R} + \vec{\omega} x \dot{\vec{R}} + \vec{\omega} x \dot{\vec{R_{NI}}} + \vec{\omega} x \dot{\vec{R_I}} \iff \tag{4.45}$$

Combining equations and

$$\ddot{\vec{R_I}} = \ddot{\vec{R_{NI}}} + 2\vec{\omega} x \dot{\vec{R_{NI}}} + \dot{\vec{\omega}} x \vec{R} + \vec{\omega} x (\vec{\omega} x \vec{R}) \tag{4.46}$$

$$\underbrace{\ddot{\vec{R_I}}}_{\text{gravity and drag force}} = \ddot{\vec{R_{NI}}} + \underbrace{2\vec{\omega} x \dot{\vec{R_{NI}}}}_{\text{Coriolis acceleration}} + \underbrace{\vec{\omega} x (\vec{\omega} x \vec{R})}_{\text{centripetal acceleration}} + \dot{\vec{\omega}} x \vec{R} \quad [25] \tag{4.47}$$

Separating in a normal and tangential force we have, and given that $\dot{\vec{R_{NI}}} = -v_d \vec{u_N}$ and $\ddot{\vec{R_{NI}}} = -\dot{v}_d \vec{u_N}$:

$$Normal : \vec{g} + \frac{\vec{Fa_N}}{M} = (-v_d + \omega^2 R)\vec{u_N} \tag{4.48}$$

$$Tangential : \frac{\vec{Fa_T}}{M} = 2\vec{\omega}(-v_d) + \dot{\vec{\omega}} \vec{R} \tag{4.49}$$

Where give us the following normal and tangential acceleration:

$$\dot{v}_d = g - \frac{Fa_N}{M} - \omega^2 R \tag{4.50}$$

$$\dot{\omega} = \frac{1}{R}(2\omega v_d + \frac{Fa_T}{M}.\vec{u_T}) \tag{4.51}$$

Re-entry	
Descent velocity (Y(1))	$-v_d(m/s)$
Angular velocity (Y(2))	$\omega\ (rad/s)$
Normal component of acceleration (Y(3))	$-an - \frac{\omega^2}{r}$
Tangential acceleration (Y(4))	$\frac{at+2vd\omega}{r}$

Table 4.4: Start conditions for the de-orbiting control

Knowing the parameters form the Table 4.4, it is possible to describe the new values for the altitude, angular position and velocities.

4.4.3 Orbits Cycle

For simulation purpose, an estimation of the number of satellite orbit to reach the release spot. The period that Earth take to complete one orbit is calculate:

$$T = 24 - \frac{24}{365} \approx 23,93\,(hours)$$

$$T = 24h - \approx 1435,8\,(minutes)$$

The satellite take between 90 to 100 minutes to complete one orbit relatively to the Earth. There so the number of orbits that will take it to reach the same spot is given by:

$$\frac{1435,8}{100} < Orbits < \frac{1435,8}{90}$$

$$14,36 < Orbits < 15,95$$

Considering that the satellite pass over the same area of release 2 times, one on the descended trajectory and other on the ascendant.

There so is estimated that the adjustment of the satellite position need to be made at each multiple of 7/8 of orbits.

4.4.4 Control Cycles

The control is organized in consecutive control cycles of 30 minutes each. This time is one control cycle. At the beginning each control cycle GPS readings are taken. Based on the position data the algorithm projects the further decent of the capsule. The purpose of this simulation is to

analyze the relative distance of the satellite to the release area. The release area is the part of the orbit from which the released capsule will land in the desired landing area without further control interactions by the operator. To do this the satellite will calculate the distance of itself from the release area while passing the release height of 110 Km. Based on this the time of control is calculated. This time will further be called T_{on}. T_{on} in this reference is the time that the larger side of the satellite is exposed area. This method is called differential drag.

4.4.5 Differential Drag

The purpose of differential drag is to influence the relative position of two satellites (or a satellite and a desired spot on the descent path). This is done by altering the drag that effects the satellite. This change in drag will then alter the orbital velocity of the satellite and thus change the position relative to an unaltered satellite. The simplest way to alter the drag is by exposing different sized front areas into the flight direction. In the case of GAMASAT the difference between the small and the large front area is a factor of three.

How it works:

While falling, the potential energy of the orbit (E_{pot}) is changed into kinetic energy (E_{kin}) and the satellite increase its orbital velocity (the overall energy is still lower). By exposing the larger surface the drag is increased. Therefore the satellite is decelerated and thus its overall energy is decreased ($E_{pot} + E_{kin}$). In result the satellite will falls faster to the ground.

Hence relative to an unaltered satellite (or the release area) the satellite will overshoot. This results in a seemingly paradox situation that decelerating the satellite will make it catch up with the release area and accelerating thereby increasing the orbit and decreasing the velocity will make it fall back. As a starting point the algorithm will calculate the T_{on}: time changing the values between 0 and 25 minutes. Based on this the new distance to the release area is projected. The calculation is based on the assumption that all follow on next T_{on} will be 25% of the 30 minutes cycle.

This value represents a set average during the mission and represents the unaltered state.

4.4.6 Implementation in the capsule

Based on the described function the algorithm calculates the T_{on} time. The largest control effect would be achievable with a T_{on} time equal half the control interval. However since this would decrease the time that the satellite stays on orbit and thus reduces the amount of science data a more moderate approach was chosen. Therefore a preset value of 25% for T_{on} was chosen. This is an optimum between the ability to control (T_{on} = 50%) and the time to stay on orbit (T_{on} = 0%).

Simulations have shown that a calculation of T_{on} takes approximately 5 seconds. In order to allow the usage of lower power micro controller in the capsule this time has been increased to 5 minutes. This would allow to use a 60 times slower micro controller.

4.5 Simulation Results

Beside considering a density variation of 50% the simulation was made for different angular positions to test the robustness of the algorithm. From the results of the Tables A.1;A.3; A.5 and A.7 following the graphics that shows the time variation (T_{on}) for the exposure area A2 and the evolution of the satellite orbit to reach a multiple of 7, for $\theta = 0; 2\pi 0,3; 2\pi 0,6$ and $2\pi 0,9$:

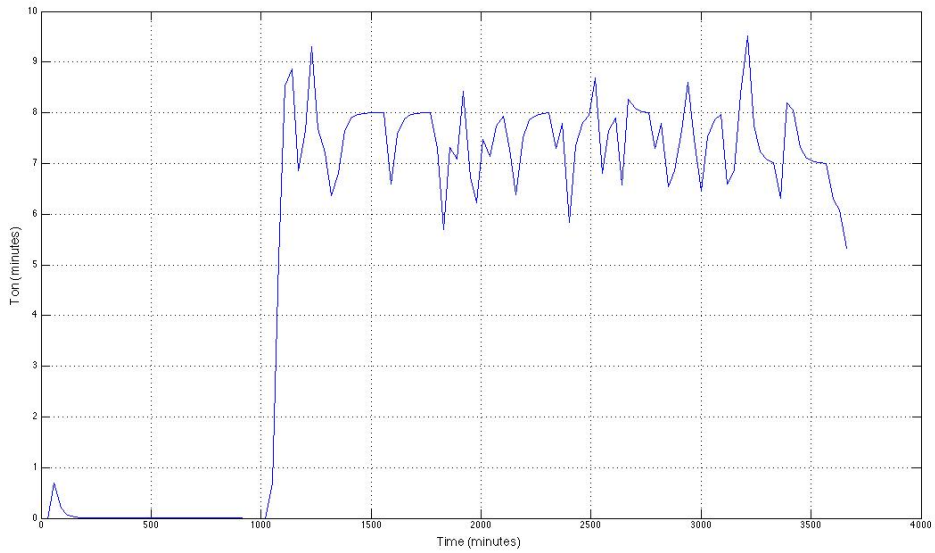

Figure 4.15: T_{on} variation with time: $\theta = 0$

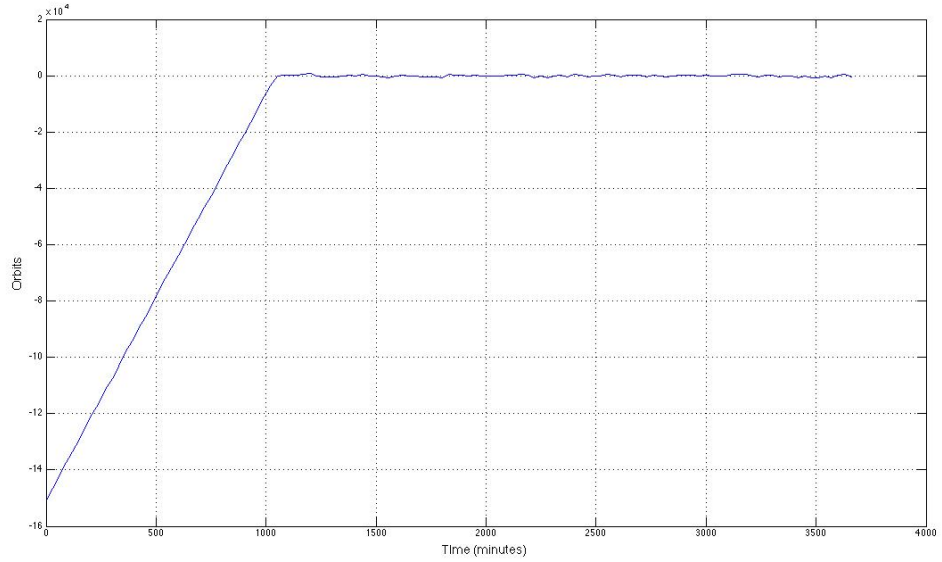

Figure 4.16: GAMASAT Orbit variation with time: $\theta = 0$

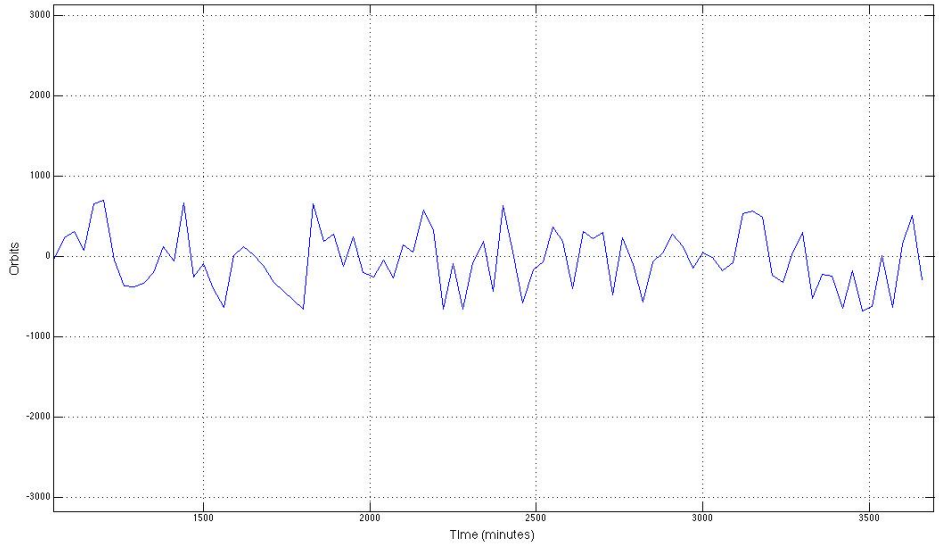

Figure 4.17: Zoom from 1100 and 2600 minutes of figure 4.16

For a $\theta = 0$ the capsule landed at a distance 299,8 (km) from the landing spot

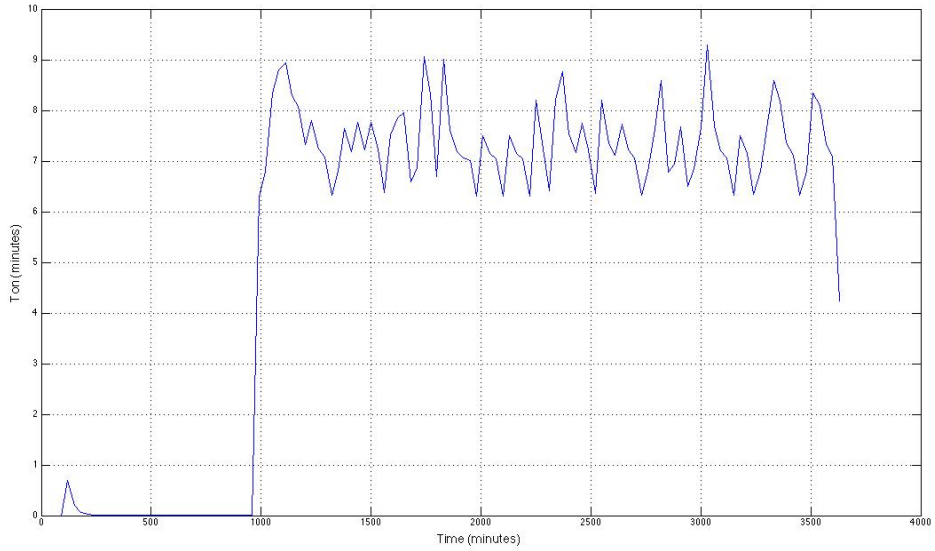

Figure 4.18: T_{on} variation with time: $\theta = 2\pi 0,3$

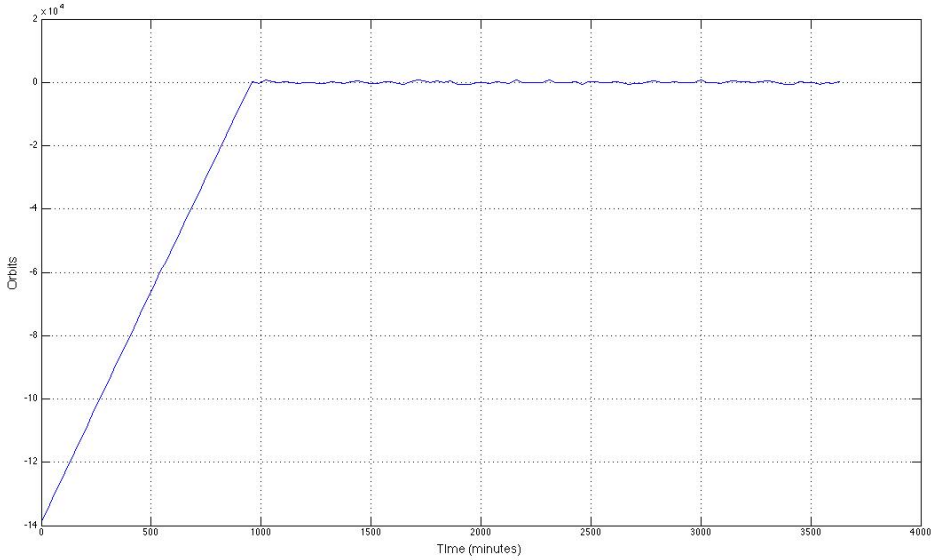

Figure 4.19: GAMASAT Orbit variation with time: $\theta = 2\pi 0,3$

For a $\theta = 2\pi 0,3$ the capsule landed at a distance 214,37 (Km) from the landing spot.

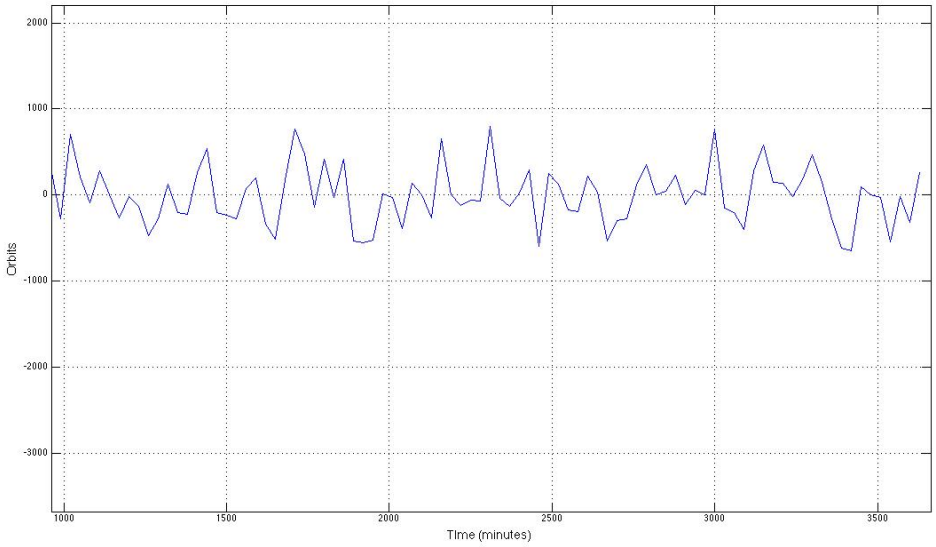

Figure 4.20: Zoom from 1000 and 2400 minutes of figure 4.19

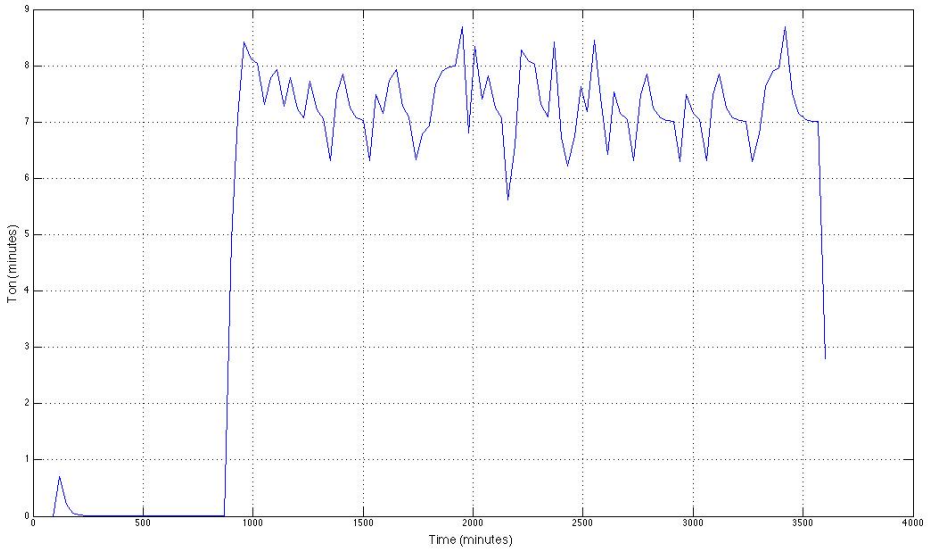

Figure 4.21: T_{on} variation with time: $\theta = 2\pi 0,6$

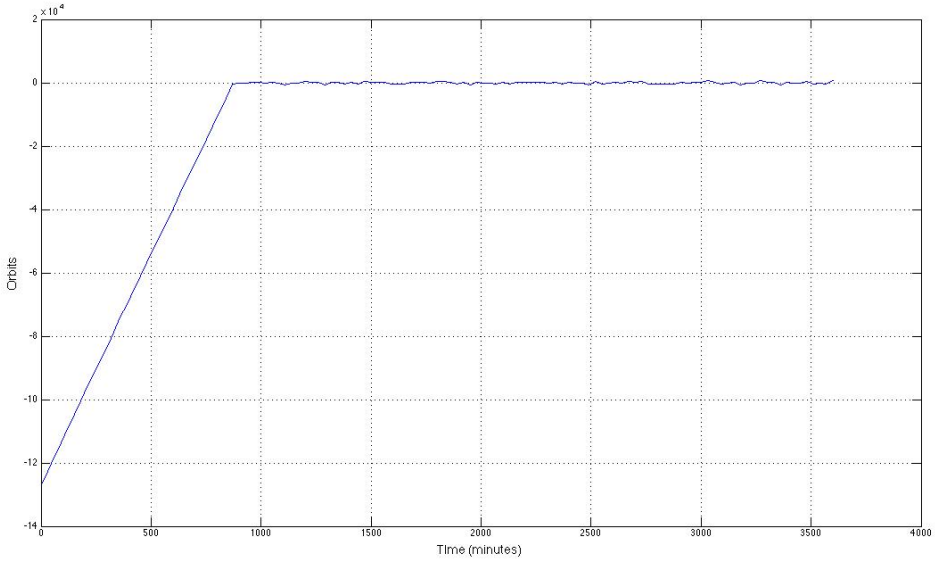

Figure 4.22: GAMASAT Orbit variation with time: $\theta = 2\pi 0,6$

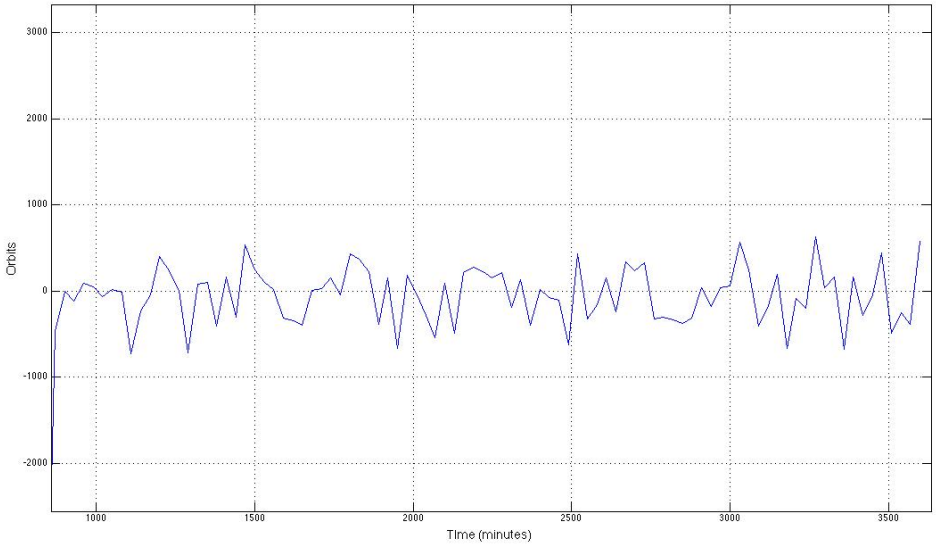

Figure 4.23: Zoom from 360 and 2400 minutes of figure 4.22

For a $\theta = 2\pi 0,6$ the capsule landed at a distance 445,07 (km) form the landing spot.

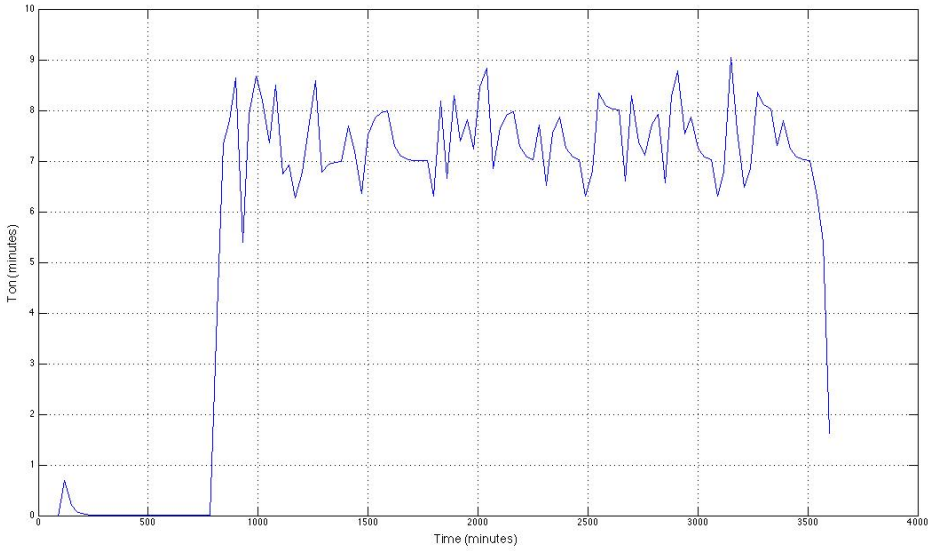

Figure 4.24: T_{on} variation with time: $\theta = 2\pi 0,9$

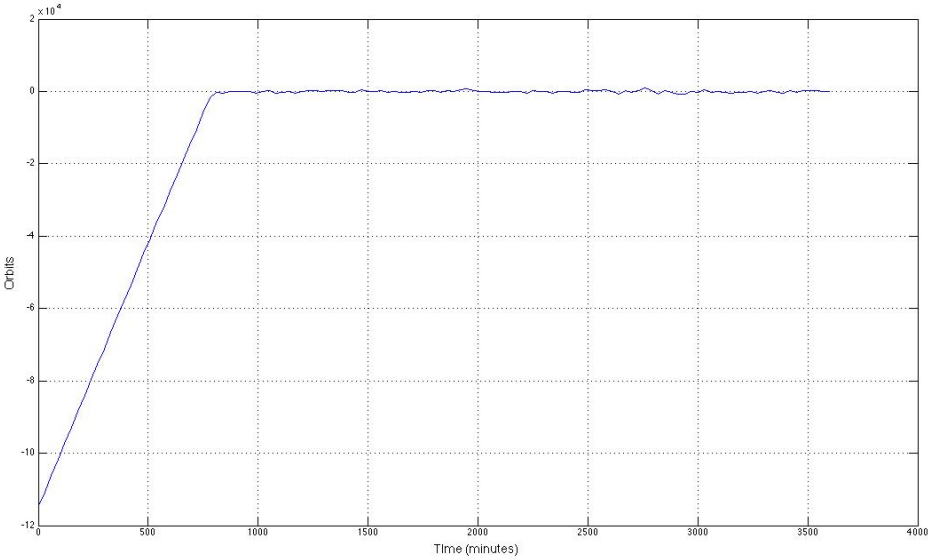

Figure 4.25: GAMASAT Orbit variation with time: $\theta = 2\pi 0,9$

For a $\theta = 2\pi 0,9$ the capsule landed at a distance 67,23 (km) form the landing spot.

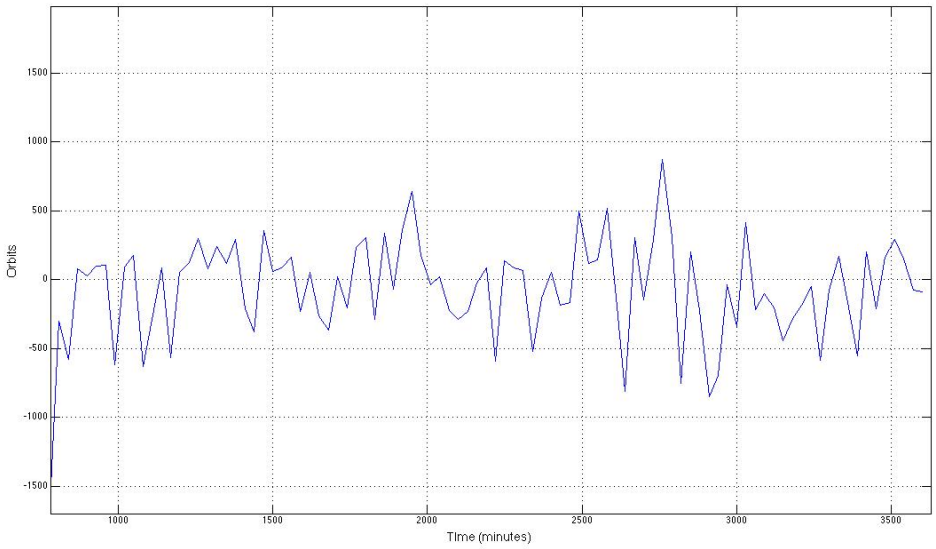

Figure 4.26: Zoom from 250 and 2400 minutes of figure 4.25

4.6 Conclusion

Based on the model for the Atmosphere density and that the satellite need to be at a multiple of 7 orbits the results showed that the estimation of 25% for the time of control is enough to maintain the orbits of the satellite closer to the release window of the capsule. After the 110 km the distance to landing spot has an error of -/+ 500 km. Despise being a simulation result, there so the results showed that the purpose of this project can be achieved.

Chapter 5

Capsule Design

Based on the positive results from the de-orbit control the next question is whether releasing the capsule at the planned spot is enough to guarantee arrival in the projected landing zone. Therefore this chapter focuses on the capsule layout and its effects of re-entry stability. Namely potential oscillation of the capsule during re-entry presents a potentially severe hazard and needs to be taken care of.

Another differentiator from existing capsule designs is that, keeping in mind its size limitations, it will not offer any further means to decelerate.

5.1 Introduction

The aim of the GAMASAT re-entry capsule is to prove the design of the first CubeSat based return capability from orbit. Therefore the mission has three main stages:

- Collect data during the GAMASAT de-orbiting
- Insure the survival after re-entry
- Land the projected landing zone.

The capsule will carry electronics that will collect data during re-entry. They are furthermore responsible to establish and maintain communication with the satellite operators on ground.

As a starting point of this work a number of requirements have been identified for the re-entry capsule of the GAMASAT mission. These requirements have been laid out in Table 5.1 and Table 5.2. The following nomenclature is used: all requirements with with 'shall' are absolutely mandatory, all requirements with should, are desired but not required requirements.

Then we have the initial conditions for the satellite:

Request ID	Name	Description
001	Data Collection	The capsule shall be able to collect data during the de-orbiting
002	Communication with Earth	The capsule shall be able to communicate with others satellite through the S band
003	Capsule Detached	The capsule shall be able send signal when the capsule is detached form the satellite and start the re-entry process

Table 5.1: Capsule Mission during the GAMASAT de-orbiting

Request ID	Name	Description
001	Survive the re-entry	The capsule shall be able survive the re-entry thermal condition
002	Oscillation Stabilization	The capsule shall be able to stabilize the oscillation due the re-entry transonic speeds
003	Land with 15J	The capsule will land with a maximum of energy of 15 J or guarantee that land on water
004	Floatable capsule	The capsule shall be able to float
005	ARGOS Communications	The capsule shall be able to communicate via UHF ARGOS messages
006	Safety of the devices	The capsule shall guarantee the safety of the devices during the re-entry process and after it land on land or water

Table 5.2: Requirements - Capsule Mission during re-entry

5.2 Design Requirements

The first care in the stabilization method was the design. The only information that we had was that all the blunt nose are dynamically unstable and the back side of the capsule had no influence on the unsuitability/stability, and therefore the presented design is based on the most successful and revolutionary designs, the Apollo 11 re-entry capsule.

5.3 Reference Capsule Design

The capsule of GAMASAT uses the proven form of the Apollo 11 capsule. The decision to take this particular capsule design was chosen before the start of this study by the experts of the GAMASAT team.

Request ID	Name	Description
001	Apollo 11 design	For a stranding point the capsule will have the same design as the successful Apollo 11;
002	3mm minimum of thickness	To give some structure to the materials, each layers will have to have at least 3 mm of thickness;
003	Battery Charging System	The top of the capsule need to lets the solar energy pass to the inside of capsule to supply the batteries and still resist to the thermal heat;
004	Fit on 1U CubeSat	Need to be smaller enough to fit inside of 1U of the GAMASAT and leave space for the deployment system, reaction wells and de-orbit control microprocessor;
005	Minimum of electronics	Is needed that inside of the capsule can fit at least 4 pcb, 3 antennas, 3 led, 2 batteries and a damper
006	More electronics	Between the 4 pcbs it is needed to leave space for more electronics devices;
007	Floatable	The majority of the capsule weight need to be below the center of mass to guarantee that will respect Archimedes Principle been able to float and to guarantee the stability and that the capsule will remain in the right position
008	Distance between the electronics and layers from the bottom	The electronics need to be distance form the inside layer to guarantee an oscillation freedom of +/-20 degrees without hit the protector layer;
009	Detachment away from thermal exposure	The opening and detachment need to be made away from the area of most thermal exposure
010	Electronics is attached to the top	The internal oscillation will only be made mass below the center of mass, there so the electronics will be supported on the top of the capsule
011	Protect from the thermal conduction	The electronics devices will be fix to top of the capsule to minimize the thermal conduction
012	On the top will be placed 3 antennas	For communication purpose will be placed 3 antennas on the top of the capsule and above the sea level when landed it on water.

Table 5.3: Design requirements

5.4 Material Selection

Fiber reinforced silicon carbide (CSiC) is a potential non ablative solution. It has a low coefficient of thermal expansion and is therefore a good substitute for the cork P50. However the carbon fiber inside the CSiC structure increases both electrical as well as thermal conductivity. In result there is the risk to damage the internal devices.

Air friction during re-entry is a significant source of heating. Therefore a thermal protection

system is necessary for the capsule. Research indicates that cork P50 is a successful thermal protector [28]. It is therefore commonly used in spacecraft booster nose cones. The source of its good thermal protection is a slow ablative cooling process. However do to the small size of the capsule and the severity of the heat induced in the ablative process of re-entry, the inert a still threatened to burn. Therefore a non-ablative heat protection system would be preferable. Fiber reinforced silicon carbide (CSiC) is a potential non ablative solution. It has a low coefficient of and is therefore a good substitute for the cork P50. However the carbon fibre inside the CSiC structure increases both electrical as well as thermal conductivity. In result there is the risk to damage the internal devices.

5.4.1 Cork Composite- P50

Due to its cellular structure cork is both extremely light and resistant. It possesses a very high coefficient of friction and is a poor conductor of electricity, sound and heat. It furthermore has an exceptional shock-absorbing capacity;

This extra ordinal combination of properties make cork an ideal material for a wide range of applications [27].

Refinement in the fabrication process the cork P50 further increases these properties and make it one of the best thermal protection materials for the aerospace purposes [28]. More detail about this cork can be seen the following Table:

Properties	
Density (max)	$512(kg/m^3)$
Thermal conductivity	0.07 (W/m.K)
Specific Heat	$2.1(kJ/kg.K)$

Table 5.4: Main properties of the cork P50 ACC based TP

5.4.2 Carbon fibre-reinforced silicon carbide (C-SiC)

Silicon carbide is a compound of carbon and silicon atoms in a of tetrahedral structure. Its strong bonds in the crystal lattice make it one of the hardest materials second only to diamond. High thermal conductivity coupled with low thermal expansion and high strength gives this material exceptional thermal shock resistant qualities. Another of the C/SiC properties is its high elastic modulus, low density and superior chemical inertness[29].

Due to its characteristics SiC was first used as an abrasive for industrial and optical processing. In the recent time it furthermore became attractive in a number of high performance applications using a sinter process. Today SiC can be found in ball valve parts, heat exchangers, semiconductor process equipment, suction box covers, turbine components and hot gas flow liners 1, brake disks and pads with high performance vehicles as well emergency brake systems with high and stable

coefficients of friction and low wear rates [2]. In the frame of this project mainly its thermal properties are of high interest.

			CVI		LPI		LSI	
			C/SiC	C/SiC	C/SiC	C/C-SiC	C/C-SiC	C/SiC
Manufacturer			SPS (SNECMA)	MT Aerospace	EADS	DLR	SKT	SGL (9)
Density		g/cm^3	2.1	2.1 - 2.2	1.8	1.9 - 2.0	> 1.8	2 / 2.4
Porosity		%	10	10 - 15	10	2 - 5	-	2 / <1
Tensile strength		MPa	350	300 - 320	250	80 - 190	-	110 / 20-30
Strain to failure		%	0.9	0.6 - 0.9	0.5	0.15 - 0.35	0.23-0.3	0.3
Young's modulus		GPa	90 - 100	90 - 100	65	50 - 70	-	65 /20-30
Compression strength		MPa	580 - 700	450 - 550	590	210 - 320	-	470 / 250
Flexural strength		MPa	500 - 700	450 - 500	500	160 - 300	130 - 240	190 / 50
ILSS		MPa	35	45 - 48	10	28 - 33	14 - 20	-
Fibre content		Vol.%	45	42 - 47	46	55 - 65	-	-
CTE Coefficient of thermal expansion	∥	10^{-6} K^{-1}	3(1)	3	1.16(4)	-1 - 2.5(2)	0.8-1.5(4)	-0.3 / 1.8 (5)
	⊥		5(1)	5	4.06(4)	2.5 - 7(2)	5.5-6.5(4)	-0.03–1.36 (6) / 3 (7)
Thermal conductivity	∥	W/mK	14.3-20.6(1)	14	11.3-12.6(2)	17.0-22.6(3)	12 - 22	23–12 (8) / 40-20 (8)
	⊥		6.5 - 5.9(1)	7	5.3 - 5.5(2)	7.5 - 10.3(3)	28 - 35	
Specific heat		J/kgK	620 - 1400	-	900-1600(2)	690 - 1550	-	-

∥ and ⊥ = Fibre orientation; (1) RT - 1000 °C ; (2) RT - 1500 °C; (3) 200 - 1650 °C; (4) = RT - 700 °C; (5) 1200 °C; (6) 200 – 1200 °C; (7) 300 – 1200 °C; (8) 20 °C – 1200 °C; (9) values for fabric/short fibre reinforced material

Table 1. Typical material properties of C/SiC and C/C-SiC materials in dependence of the manufacturing method.

Figure 5.1: CSIC specifications [30]

5.4.3 Vacuum

At the molecular level, heat is the result of the energy transfer between molecules motion and a surface. The faster the molecules move, more energy is transfer from the hotter to the cold. The heating can be made by three ways:

- Conduction is made by transferring the energy though collision between the faster moving molecules, hotter, and the slow moving particles, colder. This collision causes the increase of speed on slow particles and consequently become hotter. In case of vacuum, there is no particles to collide with, there so the heating cannot be made by conduction.
- Convection is the case when a moving substance such as air or water. A source of heat (such as a heater in a home) heats the air around it and blows it out into the room. As it flows out into the room, it rises and pushes colder air down and back to the heater. This cool arm is warmed and the process repeats. Since there's no substance in a vacuum to move, heat transfer through a perfect vacuum via convection is impossible.
- Radiation is when the heat is transferred by the spread of electromagnetic waves, like sun light. Some of these light waves strike molecules of air and cause them to speed up. Since

electromagnetic waves are not impeded by a vacuum, heat can be transfer through a vacuum via radiation.

5.5 Capsule layout

The capsule was designed using Solidworks. It has a conical shape with a blunt nose and a rounded top. The capsule has diameter of 95 mm and a height of 55 mm and an side angle of $\approx 33°$. As explained earlier the capsule uses a thermal shield made of two thermal protectors, cork P50 and CSiC. The outer shell is made off cork P50 which is placed as a thick structure for ablative cooling material. Furthermore inside the capsule is a second layer made of CSiC. This material prevents the burning of the electronic devices. Since CSiC is a good thermal protector a third layer of thermal insulation is used. This layer between the CSiC heat sink and the electronics is vacuum/air.

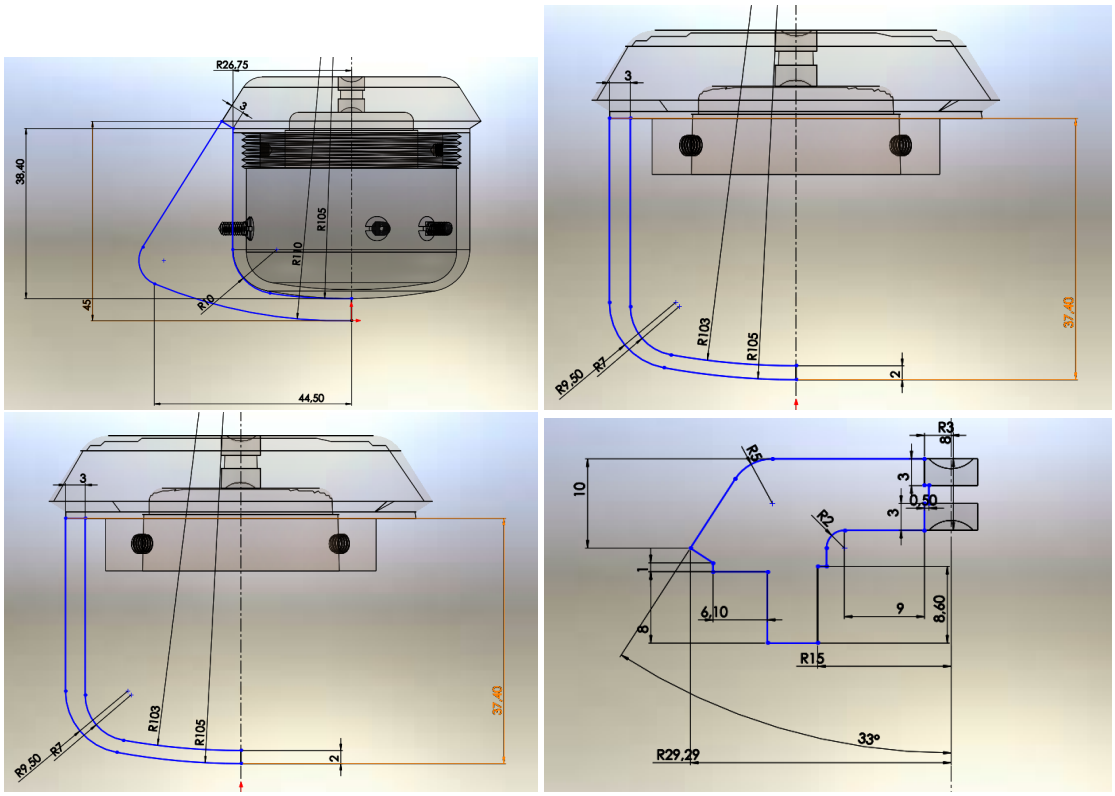

Figure 5.2: Capsule layout

5.5.1 Floatability

As one of the requirements, 3 antennas will be placed on the top of the capsule for communication purposes. This will keep them of being outside of water and compromise the communication. To do so, the Archimedes Principle law will be used to guarantee the floatability.

$$M_C = V_{DV}\,\rho_{sea} \tag{5.1}$$

In order to guarantee that when landed it on water the top of the capsule will not be submerge, the mass of the capsule was bounded by the Archimedes Principle so that the floatation line is bellow the antenna layer Using the *Mass properties*, from Solidworks it was possible to get a volume of $\approx 186\ cm^3$ considering a water density of $\rho = 1g/cm^3$ the minimum capsule weight is $\approx 186\ grams$.

5.6 Final layout

Not having a guideline for the design of the capsule and not being possible to test it before the launch, the fact of being designed based on the Apollo 11 and made of the most reliable materials, cork P50 and C-SIC , for extreme conditions, there are good chances that the capsule will survivor the re-entry process. As it can be seen in Table 5.5 the capsule design fulfills all initial design requirements.

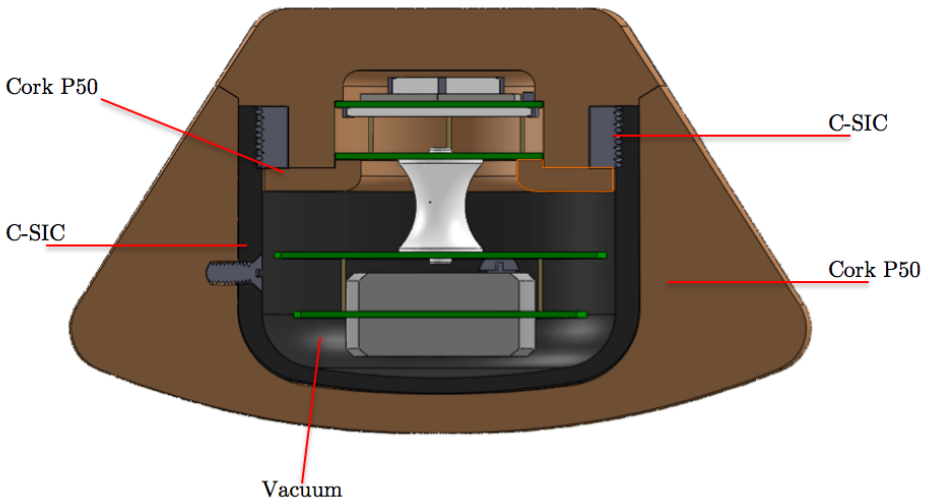

Figure 5.3: Capsule layers

Request ID	**Name**	**Description**
001	Apollo 11 design	The capsule as a resized model of Apollo 11[31]
002	3 mm minimum of thickness	Each layers will have 3 mm of thickness
003	Battery Charging System	On the top of the cover will be placed a concave and a convex lens. Each one with 3mm diameter. This allow reflect light inward to the convex and then reflect on the solar panel;
004	Fit on 1U CubeSat	55mm x 95 mm
005	Minimum of electronics	4 pcb, 3 antennas, 3 led, 2 batteries and a damper
006	More electronics	Check
007	Floatable	Check
008	Distance between the electronics and layers for the oscillation stabilization	+/-20 degrees of freedom for internal oscillation
009	Detachment away from thermal exposure	Check
010	Electronics is attached to the top	Check
011	Protect from the thermal conduction	Check

Table 5.5: Compliance Matrix

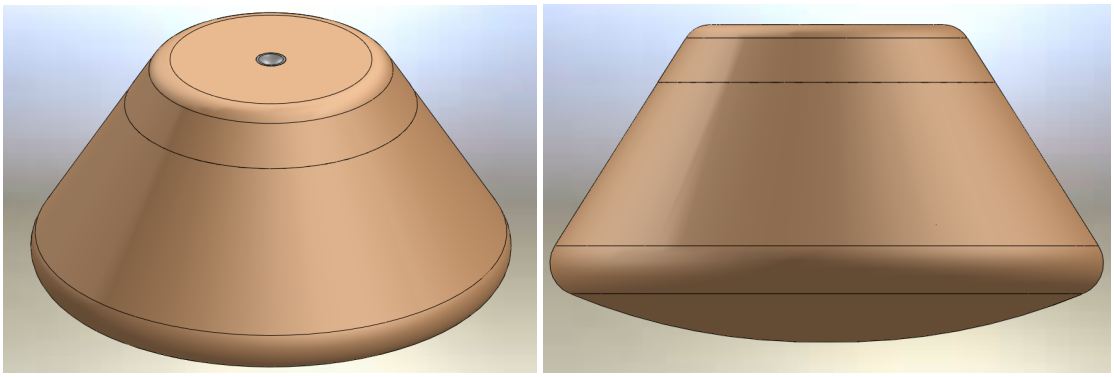

Figure 5.4: Capsule layout - top (left) view; front view(right)

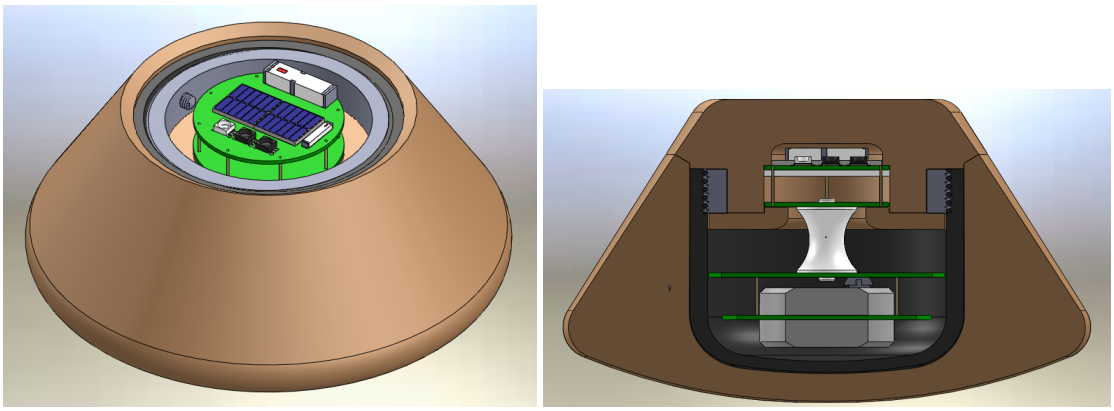

Figure 5.5: Capsule layout - Cover Detached(left); Transversal view (right)

Chapter 6

Re-entry Stability

The greatest threat to survivability of the capsule is unstable oscillation during re-entry. All the care to release it at the ideal altitude and location as well as thermal protection design as well proper selection of materials are in vain if the capsule make the re-entry in an unstable condition.

Previous studies showed that capsule with blunt nose are pre-determined to be dynamically unstable at transonic speeds[32].

Three effects influence the capsule oscillation during de-orbit:

- **Pressure variation of the Apparent Wind**: During the re-entry the capsule is exposed to apparent wind. This apparent wind is made of the particles that impact on the structure. Since the amount of particle that impacts in an object is correlated with the pressure that means any change in particle flux will result in a change of pressure. In case the capsule jitters and thus moves different cross sections to the apparent wind this will result in a fluctuation of pressure. In effect this fluctuation of pressure will result in an oscillation of the capsule around its designated of pitch angle.

- **Exchange of pressure limited by speed of sound:** The maximum velocity that a change of pressure can travel in any fluid is the speed of sound. Therefore even with a small capsule there is a delay between a change of pressure at the front of the capsule to the back of the capsule. This delay causes a hysteresis effect and consequently makes the capsule dynamically unstable [32].

- **Turbulence behind the capsule:** Any object traveling in a fluid will create some form of turbulence in the areas where high and low pressure mix. This is similar to the wake turbulence behind an airplane wing or the shock waves behind a rifle bullet. This chaotic turbulence will create oscillation of the capsule.

Previous studies have shown that the aerodynamic characteristic of the capsule depends mainly on the capsule front moment. It can also be said that the effects on the backside of the capsule can be considered as the front moment with a delay due to speed of sound[32].

Therefore two main methods where chosen to stabilize the re-entry: First is to modify the design of the capsule in a way that it supports

6.1 Stabilization Method

To stabilize the oscillation the capsule will carry a rubber damper that act as a spring and shock absorber. This system will place between the electronics devices and the capsule.

The rubber connector will act both as a damper and a spring. The spring will have a regenerative effect and will make the rubber return to the resting position. The damper will reduce the internal oscillation that is caused by the external oscillation.

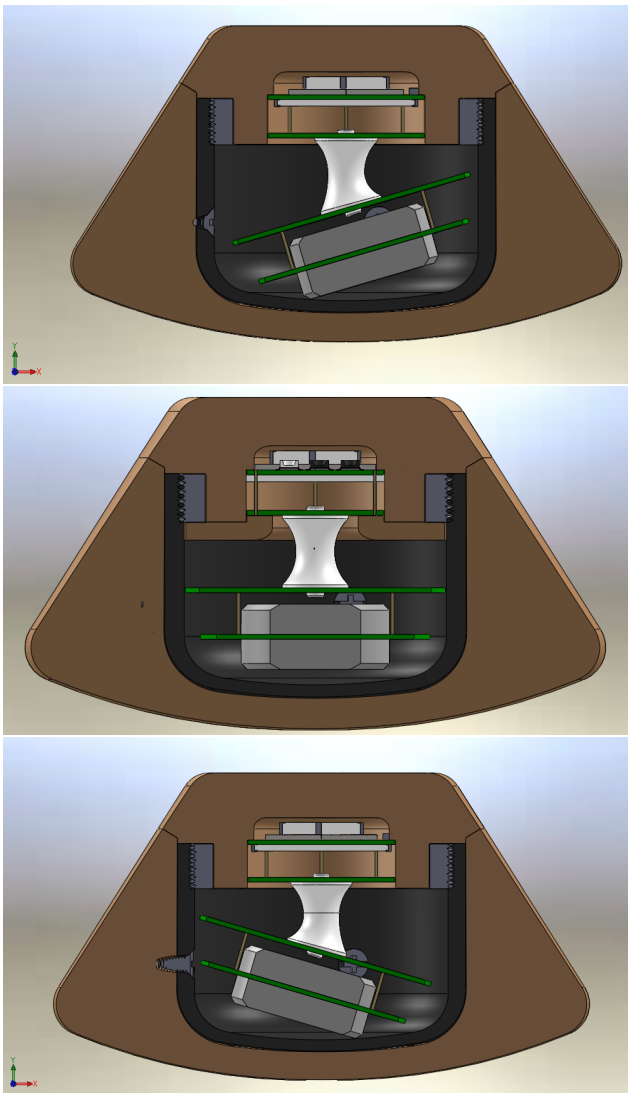

Figure 6.1: Oscillation - rubber effect

6.2 Calculation of Re-entry Stability

Rubber was chosen as damper material due to its simplicity. A rubber damper can be build in the confined space of the capsule and it can smoothly reduce the internal oscillation.

In order to chose the right rubber material an simulation was performed.

The analysis is based on the evaluation of the torque introduced into the system by both the external oscillation and the the rubber damper:

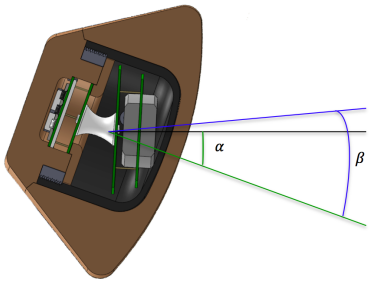

Figure 6.2: Pitch angle (α) and internal angle due the rubber (β)

As explained earlier the rubber damper will work as spring and a damper, therefore the internal torque is describe by:

$$T_i = \underbrace{k_s\beta}_{\text{spring torque}} + \underbrace{k_d\dot{\beta}}_{\text{damper torque}} \quad (Nm/s)[25] \tag{6.1}$$

The external torque causes an internal torque. This torque correspond to the acceleration of the internal mass:

$$T_i = I_m(\ddot{\alpha} + \ddot{\beta}) \tag{6.2}$$

The rubber damper will counter the capsule movement, there so the relation between the equation 6.1 and 6.2 is:

$$-(k_s\beta + k_d\dot{\beta}) = I_m(\ddot{\alpha} + \ddot{\beta}) \tag{6.3}$$

Applying the Laplace transformation:

$$-k_s\beta(s) - sk_d\beta(s) = I_m s^2(\alpha(s) + \beta(s)) \iff (I_m s^2 + k_d s + k_s)\beta(s) = -I_m s^2\alpha(s)$$

From the equation above comes the relation between external and internal angle:

$$\beta = \frac{-I_m s^2}{(I_m s^2 + k_d s + k_s)}\alpha(s) \tag{6.4}$$

Apply Laplace transformation in the equation 6.2 and substituting β for the equation 6.4 in:

$$T_i = I_m(\ddot{\alpha}(s) + \ddot{\beta}(s)) \iff T_i = s^2 I_m(\alpha(s) + \beta(s)) \iff$$

$$T_i = s^2 I_m(1 - \frac{I_m s^2}{I_m s^2 + k_d s + k_s})\alpha(s) \iff$$

$$T_i = s^2 I_m \frac{k_d s + k_s}{I_m s^2 + k_d s + k_s}\alpha(s) \tag{6.5}$$

External Torque:

$$T_e = T_i + I_M \ddot{\alpha} \tag{6.6}$$

Laplace transformation:

$$T_e(s) = T_i(s) + s^2 I_M \alpha(s) \tag{6.7}$$

Combining both torques 6.5 and 6.7:

$$T_e(s) = s^2(I_m \frac{k_d s + k_s}{I_m s^2 + k_d s + k_s} + I_M)\alpha(s) \tag{6.8}$$

$$T_e(s) = \frac{I_M I_m s^2 + k_d(I_M + I_m)s + k_s(I_M + I_m)}{I_m s^2 + k_d s + k_s} s^2 \alpha(s)$$

$$T_e(s) = \frac{1}{G(s)}\alpha(s) \tag{6.9}$$

with:

$$\frac{1}{G(s)} = \frac{s^2(I_M I_m s^2 + k_d(I_M + I_m)s + k_s(I_M + I_m))}{I_m s^2 + k_d s + k_s} \tag{6.10}$$

By using a rubber damper we are making the capsule return to the point before been apply the atmospheric drag force that made change the pitch angle, given by:

$$D_m(s) = -\frac{1}{G(s)} \tag{6.11}$$

$$G(s) = \frac{I_m s^2 + k_d s + k_s}{s^2(I_m I_M s^2 + k_d(I_M + I_m)s + k_s(I_M + I_m))}$$
$$G(s) = \frac{s^2 + \frac{k_d}{I_m}s + \frac{k_s}{I_m}}{s^2(I_M s^2 + k_d(\frac{I_M}{I_m} + 1)s + \frac{k_s}{I_m}(\frac{I_M}{I_m} + 1))} \tag{6.12}$$

6.2.1 Nyquist Analysis

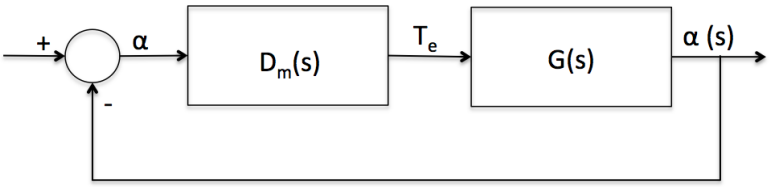

Figure 6.3: Loop System

These flow field are composed for different frequencies. Therefore it is important to analyze whether the rubber damper will be able to guarantee the stability of the system.

To do so a Nyquist stability analysis was done using Equation 6.12.

In a frequency domain comes:

$$G(j\omega) = \frac{-I_m\omega^2 + k_d j\omega + k_s}{-\omega^2(I_M I_m \omega^2 + jk_d(I_M + I_m)\omega + k_s(I_M + I_m))} \tag{6.13}$$

$$G(j\omega) = \frac{-\omega^2 + \frac{k_d}{I_m}j\omega + \frac{k_s}{I_m}}{-\omega^2 I_M(\omega^2 + j\frac{k_d}{I_m}(1 + \frac{I_m}{I_M})\omega + \frac{k_s}{I_m}(1 + \frac{I_m}{I_M}))} \tag{6.14}$$

Re-writing the 6.12 in form of

$$G(s) = \frac{1}{I_M} \cdot \frac{s^2 + 2\zeta\omega_n s + \omega_n^2}{s^2(s^2 + 2\zeta'\omega_n' s + \omega_n'^2)} \tag{6.15}$$

we have :

$$\eta = 1 + \frac{I_m}{I_M}; \quad \omega_n = \sqrt{\frac{k_s}{I_m}}; \quad \zeta = \frac{1}{2\omega_n} = \frac{k_d}{I_m} = \frac{k_d}{2\sqrt{I_m k_s}}$$
$$\omega_n' = \sqrt{\eta\frac{k_s}{I_m}} = \sqrt{\eta}\omega_n; \quad \zeta' = \frac{1}{2\omega_n'} = \eta\frac{k_d}{2\sqrt{I_m k_s}} = \sqrt{\eta}\zeta \tag{6.16}$$

Analyzing the equation above some conclusion can be take:

- The η give us the relation between external Inertia and the internal;
- The ω_n is the range of frequency that we want to analyze the capsule stability (natural frequency)
- ζ is the system damping coefficient

6.3 Capsule - Moment of Inertia

6.3.1 Internal and External Inertia

As one of the design requirements, the electronics should to be fix on the top of the capsule. Between the electronics on the bottom will be support by a rubber damper fix on the second pcb on the top. The oscillation will be relatively to the center of the rubber. The oscillation control will be made from below the center of the rubber to the electronics on the bottom and the rest will oscillate relatively of the apparent wind. We can distinguish two Moment of Inertia. One made from the oscillation of the rigid components (capsule, electronics on the top and first half of the rubber), designated as the External Inertia. The other form the controlled oscillation made by the components below the other rubber half , designed as the Internal Inertia.

Considering all the density of all the layers and components that the capsule will be made and using the tool **Mass properties** form the Solidworks was possible to reach the following properties.

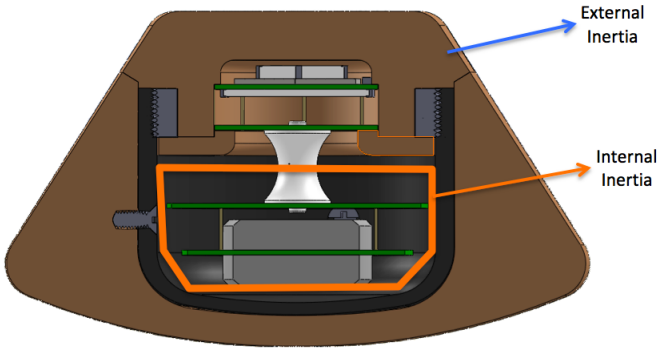

Figure 6.4: Internal and External Inertia

Full Capsule

- Coordinates of center of mass: (35,64 ; 39,85; 82,04);

External Capsule

- Weight of the rigid components: 130 $grams$;
- Coordinates of rotation point: (35,64 ; 45,01 ; 82,04);
- Moment of External Inertia : $83,4\,10^3 grams\,mm^2$

Internal Components

- Weight of the components below the rubber : 40 $grams$;
- Coordinates of rotation point: (35,64 ; 52,96 ; 82,04);
- Moment of External Inertia : $7,8\,10^3 grams\,mm^2$

From the proprieties above we can take a relation between the External and Internal Inertia of $\approx 1:10$. Relating with the $\eta = 1 + \frac{I_m}{I_M}$ from Equation 6.16, give us a $\eta = 1,3$.

6.4 Simulation Results and Analysis

Literature suggests a delay of transmission from pressure changes from the front to the back of 3 microseconds [32]. This is under the assumption that the flow field on the back of the capsule is free of perturbations. This finding was used as a starting point for the analysis. To achieve a more precise result the **nyquist** tool from Matlab was used. The **nyquist** function give us the frequency response of the system, composed by the capsule and the rubber damper.
Generated the Nyquist response on the frequency domain, an analyzes was made to find the closeted point of the diagram to the point (-1;0), for the following parameters:

parameters	
ω_n (normal frequency)	[1:20]
ζ (damping coefficient)	[0,65:1]

Table 6.1: Parameters for the Nyquist analyzes

To find the closed graphic point furthest form the point (-1;0) an analyzes of the margin of gain and frequency was made. To achieved the **margin** tool from Matlab was used. The system stability is given by how far is the graphic from the point (-1;0), therefore we selected the 10 best values for ω_n and ζ to the best solution Table 6.2.

Gain Margin (dB)	**Phase Margin (degree)**	ω_n **(Hz)**	ζ	η
7,62	25,32	9,00	0,65	1,30
7,68	21,85	6,00	0,85	1,30
7,97	24,53	8,00	0,75	1,30
8,15	19,19	5,00	0,75	1,30
8,65	22,87	7,00	0,75	1,30
8,84	21,10	6,00	0,75	1,30
8,86	23,72	8,00	0,65	1,30
9,17	18,33	5,00	0,65	1,30
10,00	22,03	7,00	0,65	1,30
10,36	20,24	6,00	0,65	1,30

Table 6.2: 10 Best solution on the Nyquist analysis

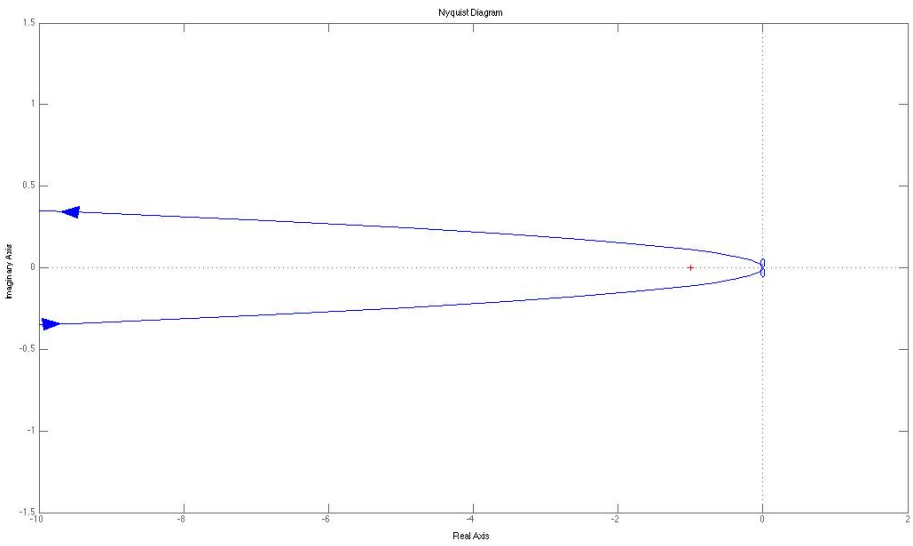

Figure 6.5: Nyquist: stability

For a $\eta = 1,3$ and given the Equation 6.16 we can take the coefficients for the rubber damper and the internal Inertia:

- spring coefficient $k_s = 0,0156 N/rad$;
- damper coefficient $k_d = 0,0101 Ns^2/rad$;
- Internal Inertia of $I_m = 0.004(kg)$

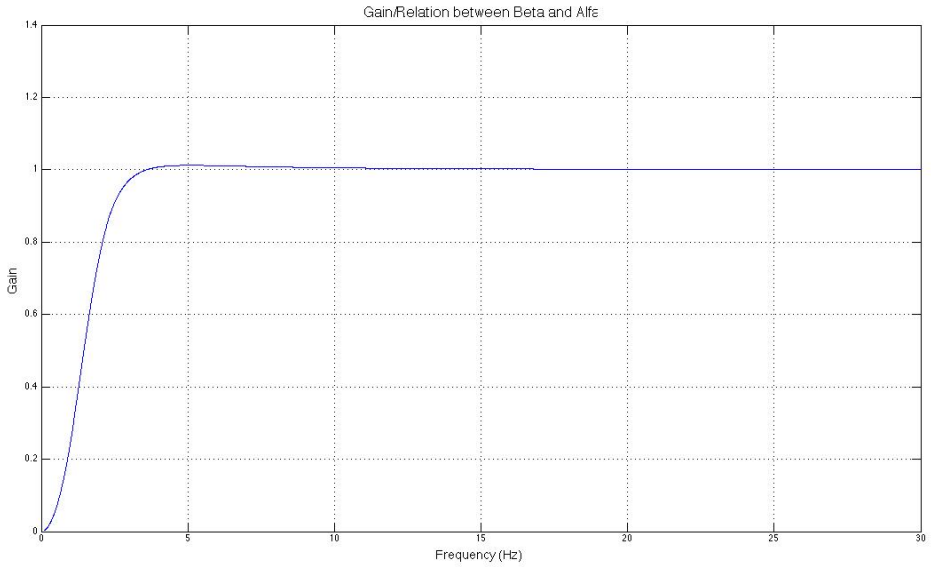

Figure 6.6: Gain between α and β

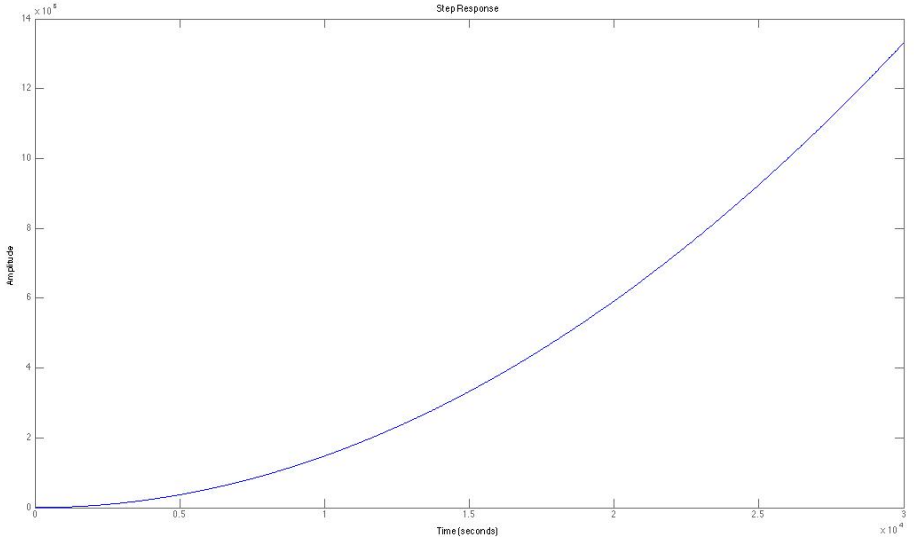

Figure 6.7: Step Response

6.5 Conclusion

The damage of the electronics devices during the re-entry is one of the main concerns. The safety of it not only depend on the thermal conditions but also the damage caused by the oscillation during the re-entry. There so the used of a rubber damper is suggested to stabilize the external

oscillation though the internal torque cause by the rubber damper. Once again the tests were made in control conditions, but give a good precision on what to expect.

Chapter 7

Future Work

When assessing the presented work two questions have been unanswered: Is the density variability very far from the reality? What are the conditions that the capsule will be exposure during the re-entry?

7.1 De-orbiting

As we saw earlier the density depend on many factors, there so an analyses of the limits of density variability is needed. The aim of this thesis was to evaluate if independently of the density variability it was possible to achieve a value for T_{on} that could guarantee a stable control and that the landing spot would be near to Portuguese EEZ. Despite achieving this goal there is the risk that depending on the density variability the actual landing area might differ from the projected zone. If this is the case the landing ray will need to be adapted. Therefore in a follow on study to this work a detailed analysis of the real world variability of atmosphere density as well as more sophisticated ways to model them in the capsule needs to be done.

7.2 Re-entry

The capsule design follows a successful row model on the re-entry process. However since the capsule is experiencing extreme thermal conditions it is necessary to further understand and model the process. Since practical experiments are difficult or impossible on ground a simulation method such as Computational Fluid Dynamics (CFD) has to be used. Only then it can be guaranteed that the cork used as an outer ablative material, despite its excellent resistance and low thermal conduction, is durable enough to withstand the re-entry process. Of particular interest is inhomogeneous burning of the cork which could lead to either a breach of the heat shield or fluctuation in the fluid due to additional turbulence created by the less smooth surface. Last but not least the burning of the cork could eventually reduce the floatability of the capsule.

Appendix A

GAMASAT Drag Coefficient

$$cos(\alpha+\beta)cos(\beta) \tag{A.1}$$

Auxiliary Calculations:

$$cos(\alpha+2\beta) = cos(\alpha+\beta)cos(\beta) - sen(\alpha+\beta)sen(\beta) \Leftrightarrow \tag{A.2}$$
$$cos(\alpha+\beta)cos(\beta) = cos(\alpha+2\beta) + sen(\alpha+\beta)sen(\beta) \tag{A.3}$$

$$cos[(\alpha+\beta)-\beta] = cos(\alpha+\beta)cos(\beta) + sen(\alpha+\beta)sen(\beta) \Leftrightarrow \tag{A.4}$$
$$sen(\alpha+\beta)sen(\beta) = cos[(\alpha+\beta)-\beta] - cos(\alpha+\beta)cos(\beta) \tag{A.5}$$

Substituting Equation A.5 on A.3 we have:

$$cos(\alpha+\beta)cos(\beta) = cos(\alpha+2\beta) + [cos[(\alpha+\beta)-\beta] - cos(\alpha+\beta)cos(\beta)]$$
$$cos(\alpha+\beta)cos(\beta) = cos(\alpha+2\beta) + [cos(\alpha) - cos(\alpha+\beta)cos(\beta)]$$
$$cos(\alpha+\beta)cos(\beta) = \frac{1}{2}[cos(\alpha+2\beta) + cos(\alpha)] \tag{A.6}$$

$$\int_{-\pi/2}^{\pi/2} \frac{1}{2} cos(\alpha+2\beta)d\beta \tag{A.7}$$
$$2\beta = \beta';\ \ 2d\beta = d\beta'$$
$$\int_{-\pi/2}^{\pi/2} \frac{1}{2} cos(\alpha+2\beta)d\beta = \int_{-\pi}^{\pi} \frac{1}{4} cos(\alpha+\beta')d\beta' = 0; \tag{A.8}$$

Time (min.)	T_{on} (min.)	≈ **Altitude** (m)	≈**vd** (m/sec)	≈ ω (rad/sec)	≈**dist0**	≈**dist1**	**orb - dbest**	≈**distance** (m)
0	0,00	200000	0,000	0,001	25,976	25,584	4,024	-160944
30	0,00	199866	0,189	0,001	26,084	25,724	3,916	-156625
60	0,00	199461	0,178	0,001	26,198	25,829	3,802	-152068
90	0,00	199338	0,006	0,001	26,310	25,928	3,690	-147581
120	0,00	199179	0,202	0,001	26,423	26,030	3,577	-143095
150	0,00	198774	0,167	0,001	26,535	26,174	3,465	-138596
180	0,00	198659	0,013	0,001	26,650	26,253	3,350	-133992
210	0,00	198473	0,215	0,001	26,750	26,382	3,250	-129993
240	0,00	198070	0,156	0,001	26,869	26,487	3,131	-125221
270	0,00	197964	0,023	0,001	26,985	26,585	3,015	-120608
300	0,00	197749	0,226	0,001	27,094	26,718	2,906	-116245
330	0,00	197352	0,143	0,001	27,213	26,831	2,787	-111472
360	0,00	197250	0,034	0,001	27,328	26,928	2,672	-106877
390	0,00	197007	0,236	0,001	27,437	27,015	2,563	-102511
420	0,00	196617	0,132	0,001	27,548	27,187	2,452	-98086
450	0,00	196518	0,047	0,001	27,668	27,290	2,332	-93274
480	0,00	196246	0,244	0,001	27,764	27,392	2,236	-89431
510	0,00	195865	0,120	0,001	27,884	27,480	2,116	-84639
540	0,00	195766	0,062	0,001	27,988	27,613	2,012	-80493
570	0,00	195466	0,251	0,001	28,108	27,706	1,892	-75677
600	0,00	195096	0,109	0,001	28,222	27,814	1,778	-71110
630	0,00	194992	0,078	0,001	28,328	27,964	1,672	-66871
660	0,00	194665	0,256	0,001	28,444	28,084	1,556	-62259
690	0,00	194308	0,100	0,001	28,559	28,152	1,441	-57655
720	0,00	194197	0,096	0,001	28,669	28,296	1,331	-53232
750	0,00	193843	0,259	0,001	28,784	28,399	1,216	-48633
780	0,00	193497	0,093	0,001	28,893	28,486	1,107	-44276
810	0,00	193375	0,113	0,001	29,003	28,611	0,997	-39866
840	0,00	192998	0,260	0,001	29,119	28,734	0,881	-35226
870	0,00	192664	0,087	0,001	29,235	28,854	0,765	-30615
900	0,00	192529	0,131	0,001	29,345	28,942	0,655	-26204
930	0,00	192130	0,260	0,001	29,447	29,067	0,553	-22137
960	0,00	191808	0,083	0,001	29,562	29,180	0,438	-17523
990	0,00	191656	0,150	0,001	29,667	29,303	0,333	-13315
1020	0,00	191237	0,259	0,001	29,785	29,417	0,215	-8615
1050	0,00	190926	0,081	0,001	29,895	29,533	0,105	-4186
1080	0,70	190755	0,168	0,001	30,007	29,645	0,001	-59
1110	5,81	190310	0,261	0,001	30,115	29,725	0,002	92
1140	8,74	189854	0,202	0,001	30,144	29,773	0,001	34
1170	8,22	189416	0,284	0,001	30,129	29,750	0,005	-197
1200	8,07	188848	0,278	0,001	30,123	29,752	0,002	63
1230	7,32	188409	0,203	0,001	30,121	29,766	0,004	-146
1260	7,10	187939	0,302	0,001	30,118	29,740	0,002	-81
1290	7,73	187350	0,283	0,001	30,117	29,742	0,006	-256

Table A.1: De-orbit Simulation -$\theta = 0$ distance from the landing point = 299.8 (km)

Time (min.)	T_{on} (min.)	≈ **Altitude** (m)	≈**vd** (m/sec)	≈ ω (rad/sec)	≈**dist0**	≈**dist1**	**orb - dbest**	≈**distance** (m)
1320	6,52	186893	0,220	0,001	30,111	29,728	0,002	62
1350	6,86	186418	0,283	0,001	30,125	29,786	0,005	213
1380	8,36	185865	0,274	0,001	30,148	29,770	0,004	165
1410	8,81	185356	0,273	0,001	30,142	29,757	0,006	256
1440	7,54	184765	0,345	0,001	30,126	29,739	0,001	-28
1470	7,86	184161	0,273	0,001	30,118	29,753	0,001	-29
1500	7,26	183662	0,281	0,001	30,119	29,709	0,006	-250
1530	7,78	183033	0,361	0,001	30,111	29,733	0,008	-339
1560	7,23	182406	0,286	0,001	30,112	29,739	0,003	-134
1590	7,07	181868	0,307	0,001	30,103	29,698	0,017	-692
1620	7,02	181196	0,377	0,001	30,103	29,711	0,004	-169
1650	6,31	180541	0,302	0,001	30,096	29,717	0,015	619
1680	6,79	180000	0,291	0,001	30,123	29,749	0,005	213
1710	8,34	179351	0,377	0,001	30,129	29,741	0,015	-593
1740	8,10	178621	0,370	0,001	30,130	29,752	0,003	137
1770	7,33	177950	0,348	0,001	30,127	29,754	0,015	591
1800	7,10	177225	0,414	0,001	30,125	29,736	0,000	-5
1830	7,73	176431	0,402	0,001	30,125	29,738	0,011	-426
1860	7,22	175689	0,391	0,001	30,122	29,739	0,008	-309
1890	7,07	174878	0,457	0,001	30,113	29,736	0,004	-179
1920	7,02	174006	0,443	0,001	30,107	29,732	0,006	-243
1950	7,01	173174	0,444	0,001	30,109	29,725	0,013	513
1980	7,00	172260	0,510	0,001	30,107	29,722	0,006	251
2010	6,30	171289	0,497	0,001	30,101	29,695	0,004	-158
2040	6,09	170405	0,441	0,001	30,117	29,734	0,004	167
2070	8,13	169472	0,543	0,001	30,143	29,772	0,019	-763
2100	8,04	168327	0,627	0,001	30,130	29,754	0,009	-367
2130	8,01	167200	0,554	0,001	30,126	29,743	0,003	-108
2160	6,60	166086	0,641	0,001	30,127	29,743	0,016	629
2190	8,28	164841	0,628	0,001	30,140	29,738	0,008	323
2220	8,78	163588	0,710	0,001	30,137	29,735	0,002	-63
2250	8,24	162066	0,868	0,001	30,123	29,749	0,012	468
2280	7,37	160522	0,732	0,001	30,117	29,748	0,004	-160
2310	7,81	159071	0,849	0,001	30,115	29,709	0,010	-416
2340	7,24	157230	1,030	0,001	30,114	29,725	0,011	-439
2370	7,07	155347	0,936	0,001	30,110	29,720	0,010	-388
2400	7,02	153437	1,111	0,001	30,108	29,734	0,008	-318
2430	7,01	151087	1,299	0,001	30,104	29,716	0,022	-863
2460	7,70	148618	1,294	0,001	30,105	29,730	0,004	-158
2490	7,21	145837	1,664	0,001	30,098	29,717	0,008	338
2520	6,36	142193	2,098	0,001	30,092	29,704	0,007	-270
2550	6,81	138036	2,268	0,001	30,115	29,754	0,000	-7
2580	6,94	132484	3,705	0,001	30,119	29,851	0,005	182
2610	2,78	121748	8,091	0,001	30,020	29,948	0,000	15

Table A.2: De-orbit Simulation -$\theta = 0$ distance from the landing point = 299.81 (km)

Time (min.)	T_{on} (min.)	≈**Altitude** (m)	≈**vd** (m/sec)	≈ ω (rad/sec)	≈**dist0**	≈**dist1**	**orb - dbest**	≈**distance** (m)
0	0,000	200000	0,000	0,001	26,279	25,913	3,721	-148839
30	0,000	199866	0,189	0,001	26,383	26,019	3,617	-144690
60	0,000	199460	0,179	0,001	26,503	26,130	3,497	-139882
90	0,000	199336	0,005	0,001	26,619	26,241	3,381	-135241
120	0,700	199179	0,202	0,001	26,721	26,337	3,277	-131099
150	0,210	198766	0,173	0,001	26,829	26,467	3,171	-126828
180	0,063	198645	0,012	0,001	26,949	26,543	3,051	-122054
210	0,019	198463	0,213	0,001	27,045	26,680	2,955	-118199
240	0,006	198051	0,164	0,001	27,152	26,769	2,848	-113927
270	0,002	197936	0,020	0,001	27,272	26,869	2,728	-109126
300	0,001	197729	0,224	0,001	27,367	27,000	2,633	-105321
330	0,000	197319	0,154	0,001	27,484	27,100	2,516	-100646
360	0,000	197208	0,030	0,001	27,599	27,200	2,401	-96047
390	0,000	196976	0,233	0,001	27,700	27,310	2,300	-92019
420	0,000	196571	0,145	0,001	27,810	27,430	2,190	-87616
450	0,000	196461	0,041	0,001	27,920	27,561	2,080	-83190
480	0,000	196203	0,241	0,001	28,022	27,648	1,978	-79109
510	0,000	195805	0,135	0,001	28,134	27,774	1,866	-74659
540	0,000	195694	0,055	0,001	28,235	27,875	1,765	-70593
570	0,000	195409	0,249	0,001	28,346	27,976	1,654	-66163
600	0,000	195019	0,125	0,001	28,457	28,048	1,543	-61707
630	0,000	194905	0,070	0,001	28,565	28,174	1,435	-57408
660	0,000	194593	0,255	0,001	28,675	28,289	1,325	-52982
690	0,000	194214	0,115	0,001	28,783	28,372	1,217	-48673
720	0,000	194094	0,087	0,001	28,892	28,496	1,108	-44306
750	0,000	193754	0,260	0,001	28,991	28,620	1,009	-40345
780	0,000	193384	0,107	0,001	29,105	28,749	0,895	-35783
810	0,000	193256	0,103	0,001	29,223	28,817	0,777	-31080
840	0,000	192890	0,263	0,001	29,324	28,941	0,676	-27054
870	0,000	192531	0,101	0,001	29,432	29,052	0,568	-22711
900	0,000	192392	0,121	0,001	29,541	29,174	0,459	-18375
930	0,000	192003	0,265	0,001	29,642	29,264	0,358	-14322
960	0,000	191654	0,096	0,001	29,752	29,371	0,248	-9913
990	0,000	191501	0,139	0,001	29,853	29,483	0,147	-5865
1020	0,000	191089	0,265	0,001	29,967	29,592	0,033	-1330
1050	2,800	190751	0,093	0,001	30,071	29,723	0,003	-102
1080	7,840	190512	0,208	0,001	30,139	29,770	0,004	-173
1110	8,652	189884	0,386	0,001	30,142	29,760	0,004	-167
1140	7,496	189334	0,184	0,001	30,114	29,707	0,009	344
1170	7,149	189014	0,216	0,001	30,111	29,721	0,001	54
1200	7,045	188418	0,366	0,001	30,102	29,719	0,010	414
1230	7,013	187873	0,187	0,001	30,104	29,744	0,008	-309
1260	6,304	187520	0,244	0,001	30,099	29,704	0,018	732
1290	7,491	186919	0,337	0,001	30,113	29,759	0,020	-786

Table A.3: De-orbit Simulation - $\theta = 2\pi 0.3$ distance from the landing point = 214.37 (km)

Time (min.)	T_{on} (min.)	≈**Altitude** (m)	≈**vd** (m/sec)	≈ ω (rad/sec)	≈**dist0**	≈**dist1**	**orb - dbest**	≈**distance** (m)
1320	7,847	186393	0,214	0,001	30,111	29,737	0,000	1
1350	7,254	185950	0,286	0,001	30,106	29,741	0,014	-580
1380	6,376	185312	0,345	0,001	30,098	29,721	0,002	74
1410	7,513	184807	0,188	0,001	30,127	29,771	0,003	-116
1440	7,154	184347	0,335	0,001	30,115	29,739	0,003	-101
1470	7,746	183620	0,367	0,001	30,116	29,744	0,009	-350
1500	6,524	183098	0,207	0,001	30,117	29,744	0,002	89
1530	7,557	182622	0,323	0,001	30,127	29,757	0,003	102
1560	7,867	181889	0,396	0,001	30,119	29,749	0,002	86
1590	7,960	181288	0,243	0,001	30,127	29,743	0,011	-438
1620	7,988	180755	0,357	0,001	30,124	29,748	0,007	262
1650	7,296	179979	0,406	0,001	30,113	29,743	0,001	-57
1680	7,089	179354	0,266	0,001	30,111	29,734	0,000	-2
1710	7,027	178753	0,397	0,001	30,109	29,702	0,012	-477
1740	7,008	177920	0,425	0,001	30,104	29,719	0,005	-213
1770	7,702	177247	0,303	0,001	30,111	29,725	0,017	-694
1800	6,511	176558	0,444	0,001	30,100	29,715	0,007	295
1830	7,553	175706	0,397	0,001	30,115	29,749	0,003	-107
1860	6,466	175004	0,381	0,001	30,116	29,727	0,009	370
1890	8,240	174190	0,456	0,001	30,127	29,754	0,006	260
1920	8,072	173296	0,469	0,001	30,129	29,765	0,004	-164
1950	8,022	172415	0,462	0,001	30,124	29,739	0,004	-171
1980	8,006	171487	0,514	0,001	30,122	29,733	0,003	-133
2010	7,302	170484	0,527	0,001	30,119	29,745	0,005	196
2040	7,091	169483	0,530	0,001	30,113	29,741	0,012	-461
2070	7,027	168417	0,587	0,001	30,113	29,727	0,011	421
2100	7,008	167272	0,603	0,001	30,112	29,729	0,001	-23
2130	7,002	166112	0,621	0,001	30,107	29,729	0,018	-737
2160	7,001	164865	0,685	0,001	30,098	29,721	0,004	142
2190	6,300	163527	0,709	0,001	30,096	29,721	0,014	551
2220	6,090	162236	0,647	0,001	30,113	29,737	0,004	167
2250	8,127	160898	0,770	0,001	30,135	29,765	0,010	-401
2280	7,338	159228	0,943	0,001	30,128	29,749	0,005	205
2280	7,338	159228	0,943	0,001	30,128	29,749	0,005	205
2310	7,801	157490	0,865	0,001	30,137	29,742	0,006	-259
2340	8,640	155761	0,990	0,001	30,120	29,737	0,007	-260
2370	6,792	153500	1,369	0,001	30,086	29,700	0,004	-178
2400	6,938	151262	0,907	0,001	30,108	29,735	0,004	152
2430	6,281	149272	1,356	0,001	30,112	29,727	0,014	553
2460	7,484	146225	1,658	0,001	30,125	29,754	0,009	-368
2490	6,445	142983	1,803	0,001	30,120	29,745	0,010	384
2520	7,534	139070	2,302	0,001	30,133	29,776	0,021	-856
2550	6,460	133378	3,736	0,001	30,133	29,846	0,004	171
2580	5,438	124141	6,266	0,001	30,069	29,954	0,004	142

Table A.4: De-orbit Simulation - $\theta = 2\pi 0.3$ distance from the landing point = 214.37 (km)

Time (min.)	T_{on} (min.)	≈**Altitude** (m)	≈**vd** (m/sec)	≈ ω (rad/sec)	≈**dist0**	≈**dist1**	**orb - dbest**	≈**distance** (m)
0	0,000	200000	0,000	0,001	26,572	26,170	1,428	-57116
30	0,000	199850	0,212	0,001	26,655	26,275	1,345	-53787
60	0,000	199384	0,215	0,001	26,726	26,349	1,274	-50951
90	0,000	199252	-0,034	0,001	26,854	26,488	1,146	-45822
120	0,000	199188	0,162	0,001	27,003	26,636	0,997	-39874
150	0,000	198772	0,209	0,001	27,125	26,744	0,875	-34997
180	0,000	198611	0,005	0,001	27,225	26,844	0,775	-31016
210	0,000	198492	0,170	0,001	27,360	26,983	0,640	-25600
240	0,000	198083	0,217	0,001	27,450	27,092	0,550	-22016
270	0,000	197904	-0,010	0,001	27,598	27,215	0,402	-16081
300	0,000	197844	0,148	0,001	27,730	27,369	0,270	-10812
330	0,000	197407	0,252	0,001	27,833	27,454	0,167	-6660
360	0,000	197198	-0,014	0,001	27,966	27,564	0,034	-1368
390	4,900	197168	0,127	0,001	28,116	27,731	0,008	313
420	6,370	196594	0,401	0,001	28,095	27,723	0,018	-732
450	7,511	196109	0,062	0,001	28,096	27,724	0,001	-42
480	2,253	195898	0,289	0,001	27,963	27,590	0,037	-1497
510	4,876	195318	0,189	0,001	28,093	27,722	0,009	347
540	7,763	195217	0,016	0,001	28,129	27,733	0,010	-381
570	5,829	194761	0,460	0,001	28,081	27,693	0,001	-39
600	8,049	194102	0,106	0,001	28,123	27,739	0,009	-341
630	4,515	194038	0,135	0,001	28,058	27,660	0,003	-101
660	3,454	193383	0,447	0,001	28,058	27,707	0,005	187
690	8,036	192994	-0,073	0,001	28,154	27,793	0,002	-87
720	11,511	193020	0,206	0,001	28,196	27,813	0,001	-46
750	5,553	192064	0,666	0,001	28,079	27,720	0,016	-631
780	3,066	191449	-0,075	0,001	28,037	27,662	0,004	-145
810	1,620	191583	0,177	0,001	28,016	27,611	0,007	-265
840	6,086	190765	0,480	0,001	28,114	27,735	0,007	-298
870	8,826	190411	-0,092	0,001	28,163	27,777	0,003	-108
900	13,148	190407	0,244	0,001	28,214	27,862	0,015	-583
930	14,444	189543	0,518	0,001	28,229	27,840	0,011	-455
960	9,233	188977	0,146	0,001	28,108	27,709	0,002	-62
990	6,970	188661	0,263	0,001	28,104	27,728	0,006	252
1020	8,391	188030	0,326	0,001	28,129	27,749	0,005	-211
1050	12,317	187696	0,042	0,001	28,221	27,815	0,017	-668
1080	5,795	187175	0,622	0,001	28,043	27,625	0,022	-862
1110	5,939	186168	0,204	0,001	28,110	27,726	0,003	114
1140	8,082	186305	-0,108	0,001	28,131	27,749	0,003	129
1170	8,024	185643	0,763	0,001	28,115	27,747	0,009	-361
1200	6,607	184520	0,194	0,001	28,109	27,718	0,002	-64
1230	10,382	184776	-0,192	0,001	28,189	27,810	0,010	-399
1260	10,815	184113	0,864	0,001	28,166	27,836	0,003	118
1290	4,644	182671	0,401	0,001	28,050	27,672	0,015	618

Table A.5: De-orbit Simulation - $\theta = 2\pi 0.6$ distance from the landing point =445.07(km)

Time (min.)	T_{on} (min.)	≈**Altitude** (m)	≈**vd** (m/sec)	≈ ω (rad/sec)	≈**dist0**	≈**dist1**	≈**30 - dbest**	≈**distance** (m)
1320	6,993	182871	-0,348	0,001	28,136	27,748	0,009	358
1350	6,998	182419	0,893	0,001	28,119	27,714	0,010	387
1380	8,399	180876	0,334	0,001	28,139	27,763	0,001	-57
1410	3,920	181019	-0,096	0,001	28,040	27,668	0,013	-518
1440	6,776	180339	0,709	0,001	28,142	27,782	0,020	788
1470	10,433	179355	0,150	0,001	28,185	27,792	0,001	-40
1500	7,330	179131	0,366	0,001	28,079	27,719	0,001	-42
1530	6,399	177944	0,666	0,001	28,094	27,729	0,004	162
1560	7,520	177354	-0,014	0,001	28,122	27,717	0,003	-127
1590	10,656	177216	0,316	0,001	28,215	27,838	0,007	262
1620	6,697	175832	1,009	0,001	28,116	27,709	0,012	494
1650	4,109	174673	0,089	0,001	28,057	27,681	0,004	175
1680	7,533	174832	0,052	0,001	28,145	27,762	0,003	127
1710	9,260	173666	1,011	0,001	28,166	27,790	0,019	757
1740	10,478	172347	0,202	0,001	28,170	27,787	0,005	195
1770	9,443	172173	0,334	0,001	28,142	27,760	0,000	4
1800	9,133	170635	1,074	0,001	28,120	27,763	0,004	150
1830	7,640	169359	0,190	0,001	28,105	27,694	0,004	162
1860	6,492	169034	0,449	0,001	28,096	27,728	0,010	394
1890	8,948	167540	0,877	0,001	28,153	27,769	0,006	-249
1920	8,284	166361	0,391	0,001	28,133	27,743	0,006	236
1950	8,085	165525	0,605	0,001	28,153	27,765	0,017	683
1980	6,626	163789	1,119	0,001	28,090	27,695	0,015	-603
2010	7,588	162317	0,318	0,001	28,126	27,754	0,001	-39
2040	9,976	161787	0,507	0,001	28,175	27,779	0,009	356
2070	7,193	159402	1,891	0,001	28,066	27,671	0,010	-411
2100	2,858	156737	0,607	0,001	28,025	27,649	0,011	450
2130	6,457	156731	-0,080	0,001	28,120	27,747	0,002	-88
2160	8,937	154857	1,944	0,001	28,163	27,763	0,005	-189
2190	5,481	151084	1,582	0,001	28,084	27,717	0,012	469
2220	7,944	149860	-0,001	0,001	28,136	27,765	0,006	221
2250	10,083	148210	2,031	0,001	28,163	27,812	0,014	-543
2280	7,225	143005	2,911	0,001	28,092	27,713	0,008	326
2310	4,967	138900	1,577	0,001	28,074	27,710	0,009	352
2340	4,290	134628	3,377	0,001	28,067	27,788	0,001	-25
2370	4,787	125973	5,417	0,001	28,069	27,912	0,004	-155

Table A.6: De-orbit Simulation - $\theta = 2\pi 0.6$ distance from the landing point =445.07(km)

Time (min.)	T_{on} (min.)	≈**Altitude** (m)	≈**vd** (m/sec)	≈ ω (rad/sec)	≈**dist0**	≈**dist1**	**orb - dbest**	≈**distance** (m)
0	0,000	200000	0,000	0,001	26,882	26,490	1,118	-44717
30	0,000	199877	0,174	0,001	27,003	26,638	0,997	-39889
60	0,000	199480	0,198	0,001	27,094	26,722	0,906	-36254
90	0,000	199338	-0,025	0,001	27,250	26,869	0,750	-29993
120	0,000	199283	0,154	0,001	27,389	27,025	0,611	-24423
150	0,000	198877	0,201	0,001	27,536	27,161	0,464	-18551
180	0,000	198740	-0,008	0,001	27,662	27,266	0,338	-13503
210	0,000	198599	0,216	0,001	27,744	27,373	0,256	-10238
240	0,000	198142	0,185	0,001	27,863	27,489	0,137	-5472
270	0,000	198069	-0,039	0,001	28,005	27,601	0,005	203
300	4,200	197905	0,267	0,001	28,082	27,706	0,003	-131
330	4,060	197229	0,323	0,001	28,060	27,672	0,007	296
360	5,418	196997	-0,037	0,001	28,075	27,725	0,001	-34
390	5,125	196811	0,309	0,001	28,073	27,684	0,011	457
420	11,338	196212	0,168	0,001	28,207	27,832	0,002	-83
450	9,001	196054	0,143	0,001	28,115	27,709	0,002	77
480	4,100	195435	0,447	0,001	28,071	27,666	0,003	138
510	1,930	194898	0,072	0,001	28,012	27,629	0,010	-386
540	4,079	194912	0,039	0,001	28,087	27,735	0,007	264
570	11,024	194490	0,337	0,001	28,215	27,829	0,002	-90
600	6,807	193837	0,326	0,001	28,084	27,690	0,001	-36
630	6,942	193497	0,043	0,001	28,102	27,738	0,002	-85
660	6,983	193279	0,258	0,001	28,112	27,732	0,010	404
690	8,395	192636	0,315	0,001	28,148	27,769	0,012	499
720	10,218	192328	0,048	0,001	28,158	27,767	0,003	-130
750	5,166	191926	0,451	0,001	28,062	27,666	0,004	-165
780	2,250	191082	0,292	0,001	28,018	27,627	0,002	76
810	2,775	190972	-0,058	0,001	28,046	27,685	0,000	0
840	6,432	190713	0,366	0,001	28,124	27,755	0,015	606
870	8,230	189910	0,333	0,001	28,152	27,751	0,003	119
900	8,069	189635	0,039	0,001	28,125	27,748	0,000	11
930	8,721	189260	0,390	0,001	28,135	27,769	0,001	-42
960	12,416	188569	0,213	0,001	28,207	27,828	0,013	-524
990	12,125	188361	0,155	0,001	28,176	27,798	0,001	50
1020	9,237	187649	0,565	0,001	28,112	27,720	0,004	-152
1050	7,671	186898	0,133	0,001	28,111	27,723	0,004	-144
1080	8,601	186845	0,096	0,001	28,125	27,753	0,004	149
1110	10,280	186163	0,541	0,001	28,166	27,763	0,024	-941
1140	11,484	185459	0,132	0,001	28,177	27,795	0,009	365
1170	7,645	185190	0,342	0,001	28,080	27,696	0,007	-261
1200	5,794	184216	0,527	0,001	28,058	27,691	0,009	-374
1230	8,038	183834	-0,105	0,001	28,127	27,761	0,004	170
1260	10,811	183746	0,360	0,001	28,178	27,813	0,002	96
1290	12,343	182678	0,554	0,001	28,214	27,824	0,007	260

Table A.7: De-orbit Simulation - $\theta = 2\pi 0.9$ distance from the landing point =67.23 (km)

Time (min.)	T_{on} (min.)	≈**Altitude** (m)	≈**vd** (m/sec)	≈ ω (rad/sec)	≈**dist0**	≈**dist1**	**orb - dbest**	≈**distance** (m)
1320	10,003	182151	0,103	0,001	28,143	27,758	0,003	-115
1350	3,701	181537	0,646	0,001	28,018	27,643	0,001	46
1380	5,310	180536	0,199	0,001	28,093	27,692	0,004	-154
1410	5,793	180472	0,102	0,001	28,077	27,707	0,007	-271
1440	7,338	179617	0,687	0,001	28,107	27,699	0,000	-14
1470	12,001	178831	0,018	0,001	28,200	27,822	0,003	-124
1500	6,400	178580	0,560	0,001	28,069	27,695	0,006	-253
1530	4,720	177073	0,708	0,001	28,055	27,660	0,014	-545
1560	5,616	176712	-0,204	0,001	28,086	27,701	0,004	-172
1590	6,585	176478	0,622	0,001	28,117	27,767	0,011	430
1620	8,275	174941	0,669	0,001	28,144	27,759	0,007	-272
1650	5,983	174396	0,070	0,001	28,088	27,706	0,001	57
1680	4,595	173752	0,679	0,001	28,083	27,683	0,011	438
1710	5,578	172394	0,539	0,001	28,090	27,692	0,014	-574
1740	6,574	171854	0,160	0,001	28,108	27,714	0,001	51
1770	5,472	170953	0,824	0,001	28,086	27,698	0,020	790
1800	8,642	169626	0,334	0,001	28,164	27,789	0,012	479
1830	3,292	168879	0,769	0,001	28,006	27,632	0,004	141
1860	3,088	167214	0,697	0,001	28,053	27,693	0,011	-448
1890	2,326	166490	0,261	0,001	28,029	27,649	0,001	-51
1920	5,598	165557	0,753	0,001	28,101	27,721	0,003	122
1950	7,979	164011	0,673	0,001	28,153	27,764	0,011	459
1980	11,494	163124	0,389	0,001	28,193	27,807	0,001	-44
2010	5,548	161341	1,611	0,001	28,058	27,678	0,002	-76
2040	5,864	158914	0,536	0,001	28,087	27,725	0,002	66
2070	8,759	158907	-0,038	0,001	28,168	27,805	0,012	468
2100	11,028	157008	1,956	0,001	28,174	27,779	0,011	-454
2130	13,108	154054	0,681	0,001	28,210	27,808	0,010	-419
2160	8,833	153050	1,191	0,001	28,110	27,732	0,002	70
2190	4,050	149162	2,383	0,001	28,054	27,665	0,010	397
2220	1,915	146171	0,818	0,001	28,013	27,648	0,010	395
2250	4,774	144695	1,207	0,001	28,082	27,725	0,011	-458
2280	9,132	140933	2,331	0,001	28,176	27,806	0,006	256
2310	12,540	136866	1,927	0,001	28,239	27,892	0,005	212
2340	11,462	130356	5,706	0,001	28,151	27,943	0,006	234
2370	3,439	111422	17,217	0,001	27,997	27,993	0,003	-114

Table A.8: De-orbit Simulation - $\theta = 2\pi 0.9$ distance from the landing point =67.23 (km)

References

[1] Qb50 project description. https://www.qb50.eu/index.php/project-description; accessed January-2013

[2] Raquel Pinho, Andrea Corte-Real, Sérgio Cunha, Pedro Rodrigues, Ricardo Mendes; A CubeSat de-orbiting and re-entry experiment; *IAA-CU-13-02-06*

[3] E Gill, P Sundaramoorthy, J Bouwmeester, and B Sanders. Formation flying to enhance the qb50 space network. In *Proceedings of the 4 Symposium, Funchal, Portugal*, 2010.

[4] Nasa launches new technology: An inflatable heat shield, 2009. http://www.nasa.gov/topics/aeronautics/features/irve.html- accessed June-2013.

[5] Inflatable re-entry vehicle experiment (irve) - 4 overview, 2011. http://ntrs.nasa.gov/archive/nasa/casi.ntrs.nasa.gov/20110012170_2011012601.pdfaccessed June-2013.

[6] Irdt with inflatable extension deployed, 2005. http://spaceinimages.esa.int/Images/2001/11/IRDT_with_inflatable_extension_deployed - accessed June-2013.

[7] The return of hatabusa went exactly according to plan - http://www.jaxa.jp/article/special/hayabusareturn/kawaguchi01_e.html - accessed june-2013, 2010.

[8] Replica of hayabusa capsule at jaxa i - http://upload.wikimedia.org/wikipedia/commons/5/51/replica_of_hayabusa_capsule_at_jaxa_i_.jpg - accessed june-2013, 2010.

[9] Asteroid explorer "hayabusa" (muses-c) capsule reentry plan - http://www.jaxa.jp/press/2010/06/20100612_hayabusa_e.html - accessed june-2013, 2010.

[10] Katharine Sanderson. Dropping a line from space. *Nature*, 449(7161):387–387, 2007.

[11] Michiel Kruijff, Erik J Van Der Heide, and Wubbo J Ockels. Data analysis of a tethered spacemail experiment. *Journal of Spacecraft and Rockets*, 46(6):1272–1287, 2009.

[12] Launch of the young engineers satellite 2, 2007. http://esamultimedia.esa.int/multimedia/edu/Press_Fact_Sheet.pdf - accessed June-2013.

[13] Michiel Kruijff. Tethers in space, a propellantless propulsion in-orbit demonstration. *Uitgeverij BOXPress, Oisterwijk*, 2011.

[14] Eelco Doornbos. Empirical modelling of the thermosphere. In *Thermospheric Density and Wind Determination from Satellite Dynamics*, pages 21–57. Springer, 2012.

[15] Wien's displacement law. http://en.wikipedia.org/wiki/Wien's_displacement_law - accessed April-2013.

[16] John Kennewell and Andrew McDonald. The solar constant. http://www.ips.gov.au/Category/Educational/The%20Sun%20and%20Solar%20Activity/General%20Info/Solar_Constant.pdf - accessed April-2013.

[17] Global climate change: Albedo. http://esseacourses.strategies.org/module.php?module_id=99 - accessed April-2013.

[18] Robert Siegel and John R Howell. *Thermal radiation heat transfer - Fourth Edition* . page 15, 2002.

[19] David A Vallado. *Fundamentals of astrodynamics and applications*, volume 12. Springer, 2001.

[20] Anders Johansen, Andrew N Youdin, and Yoram Lithwick. Adding particle collisions to the formation of asteroids and kuiper belt objects via streaming instabilities. *Astronomy & Astrophysics*, 537:7 of 17, 2012.

[21] Cristiana Monteiro Silva Ramos. Orbit calculation and re-entry control of vorsat satellite. page 66, 2011.

[22] Anders Persson. How do we understand the coriolis force? *Bulletin of the American Meteorological Society*, 79(7):1373–1386, 1998.

[23] Solar radiation. http://www.eoearth.org/view/article/156098/; June-2013

[24] Galaxy Crash Course. http://isc.astro.cornell.edu/~spoon/crashcourse.html; June-2013

[25] A.Aziz. Bazoune. Systems dynamics and control - chapter three: Mechanical systems.

[26] The cork industry in portugal. http://www.uwec.edu/Geography/Ivogeler/Travel/Portugal/cork-article2.html; accessed February-2013

[27] Cork (material). http://en.wikipedia.org/wiki/Cork_(material); accessed February-2013

[28] G. Pinaud and AJ van Eekelen. Aerofast: Development of cork tps material and a 3d comparative thermal/ablation analysis of an apollo & a biconic sled shape for an aerocapture mission.

[29] Silicon carbide, sic ceramic properties. http://accuratus.com/silicar.html; accessed February-2013

[30] Bernhard Heidenreich. Carbon fibre reinforced sic materials based on melt infiltration. In *Proceedings of the 6th International Conference on High Temperature Ceramic Matrix Composites*, 2007.

[31] Executive summary (introduction-cev): Nasa exploration systems architecture study final report (draft) october 2005, 2005. http://www.spaceref.com/news/viewsr.html?pid=19067 - accessed June-2013.

[32] Susumu Teramoto, Kouju Hiraki, and Kozo Fujii. Computationa study on the dynamic stability of bunt reenry capsule at transonic speeds. pages 30 – 56, 2001.